

New physics for muon anomalous magnetic moment and its electroweak precision analysis

^(a)Shunichi Kanemitsu and ^(a,b)Kazuhiro Tobe

^(a)*Department of Physics, Nagoya University, Nagoya 464-8602, Japan*

^(b)*Kobayashi-Maskawa Institute for the Origin of Particles and the Universe,
Nagoya University, Nagoya 464-8602, Japan*

Abstract

About 3σ deviation from the standard model prediction of muon anomalous magnetic moment (muon g-2) has been reported. We consider new physics beyond the standard model which has new Yukawa interactions with muon. We compute new contributions to muon g-2 and corrections to electroweak observables, and show the consistent region of parameter space. We find that in a simple model where the chirality flip of muon occurs only in the external muon line in one-loop muon g-2 diagrams, it is necessary to introduce the relatively large new Yukawa coupling and the electroweak scale new particles. On the other hand, in a model where the chirality flip can occur in the internal fermion line of one loop muon g-2 diagrams, we can obtain favorable g-2 contributions without large Yukawa coupling, and they are consistent with the precision electroweak observables. Finally, we discuss effects of new particles for muon g-2 on the Higgs boson decay $h \rightarrow \gamma\gamma$ and direct productions of these particles at the LHC experiment.

1 Introduction

The standard model of elementary particles (SM) has been amazingly successful, and currently the Large Hadron Collider (LHC) experiment is searching for Higgs boson, which is the only particle that has not been observed yet in the framework of the SM. So far, some interesting hints of the Higgs boson with a mass of about 125 GeV have been reported at the LHC [1] and its discovery may not be in a far future. The Higgs boson with a mass of about 100 GeV is totally consistent with the electroweak (EW) precision measurements. Therefore, the SM well-describes the nature up to the EW scale.

We, however, think that the SM is not the final theory of elementary particles. The hierarchy problem has been a strong driving force to think of the physics beyond the SM, and many ideas, such as supersymmetry, extra-dimension, and technicolor, have been proposed to solve the problem. The LHC experiment is an ideal place to probe the models for the hierarchy problem, and the searches are currently going on. The first round of the LHC searches, however, does not show any serious deviations from the SM prediction. It seems that this negative search result starts creating a tension between new physics models and the requirements for the hierarchy problem. Therefore it will be good time to consider other approaches to think about new physics beyond the SM.

There is a different approach to consider the physics beyond the SM, based on a consideration for unexplained experimental results. The muon anomalous magnetic moment (muon g-2) is one of the most precisely measured observables [2]. The theoretical prediction from the SM by several groups has suggested that there is a discrepancy between the experimental result and the SM prediction [3]:

$$\delta a_\mu \equiv a_\mu^{\text{exp}} - a_\mu^{\text{SM}} = (26.1 \pm 8.0) \times 10^{-10}, \quad (1.1)$$

where δa_μ is a discrepancy between the experimental result (a_μ^{exp}) and the SM prediction (a_μ^{SM}). There are many discussions [3, 4] on uncertainties of the SM prediction to understand whether this anomaly is real or not. If the discrepancy can not be explained by the SM, this would be an evidence of the physics beyond the SM. At present, there seems no satisfactory explanation for this anomaly within the SM. Therefore, it is worth while considering the physics beyond the SM seriously in order to explain the anomaly.

It is interesting to note that the anomaly of muon g-2 is the same size as 1-loop contributions induced by the EW gauge bosons in the SM. This suggests that in order to explain the anomaly, new particles with masses of EW scale are required if the interactions are of order of EW gauge couplings.

Although the anomaly of muon g-2 has been discussed in the context of new physics models (for example, see Ref. [5] in MSSM, Ref. [6] in extra dimension model, and Ref. [7] in Little Higgs model) motivated mainly by the hierarchy problem, we take a “bottom-up” style approach ^{#1}. Starting from introducing new interactions with muon to generate new contribution to muon g-2, we try to capture important features of new physics models, although

^{#1} See also Ref. [8] for the recent related studies.

we can only discuss a part of complete models. In this paper, we consider models where muon has new Yukawa type interactions with new particles to generate new contributions to muon $g-2$. We find that in a model where the chirality flip of muon occurs only in external line of muon $g-2$ diagrams, it is necessary to introduce the relatively large Yukawa coupling and the EW scale new particles. On the other hand, in a model where the chirality flip can happen in the internal lines of muon $g-2$ diagrams, we can obtain favorable $g-2$ contributions without large Yukawa couplings, and they are also consistent with the precision EW observables. We also expect these particles may be observed directly and/or indirectly at the LHC experiment.

This paper is organized as follows. In the next section, we consider new physics models where muon has new Yukawa couplings to explain the anomaly of muon $g-2$. One model is that only right-handed muon has new Yukawa coupling. Another one is that both right- and left-handed muons have new Yukawa interactions to enhance the contributions to the muon $g-2$. We show the consistent region of parameter space. In Sec. 3, we discuss effects of the new physics on EW observables and whether the parameter space which is consistent with the muon $g-2$ is also consistent with the precision measurements. In Sec. 4, we discuss phenomenology of these new physics models at the LHC. Especially we show the possible effect on the Higgs boson decay of $h \rightarrow \gamma\gamma$, and the direct production cross sections of new particles at the LHC. Sec. 5 is devoted to summary.

2 New physics models for anomaly of muon $g-2$

In order to explain the deviation from the SM prediction of muon $g-2$ by new physics, muon has to have new interactions with some charged particles. Since the effective operator for muon $g-2$ couples to photon, the loop effects via the new interactions of muon with charged particles could induce the extra contribution to the muon $g-2$.

In this paper, as such new interactions, we consider new Yukawa-type couplings with right-handed or/and left-handed muon. We consider two cases: (1) Model where only right-handed muon has new Yukawa interaction and (2) Model where both right-handed and left-handed muons have new Yukawa interactions.

2.1 Model where right-handed muon has new Yukawa interaction with $SU(2)$ singlet scalar (ϕ) and singlet Dirac fermion (χ)

We consider the following Yukawa interaction where the right-handed muon couples to new $SU(2)_L$ singlet fermion χ and singlet scalar ϕ :

$$\mathcal{L} = -y_N \bar{\mu}_R \chi_L \phi - m_\chi \bar{\chi}_R \chi_L + \text{h.c.} - m_\phi^2 \phi^\dagger \phi + \dots \quad (2.2)$$

Here μ_R is the right-handed muon. QED charges of new fermion χ and scalar ϕ are Q_χ and $Q_\phi = -1 - Q_\chi$, respectively, in order to have the gauge invariant Yukawa interaction. The masses of χ and ϕ are denoted by m_χ and m_ϕ , respectively. In order to simplify the model,

we have assumed a Z_2 parity, under which the SM particles are even and new particles ϕ and χ are odd. This type of the parity may be interesting for the dark matter. We also note that even if we impose the Z_2 parity, the right-handed electron, for example, can have similar Yukawa interaction with ϕ and χ . This will cause severe flavor mixing problem. We will not discuss the complete model here, however, we implicitly assume that χ or ϕ has approximate muon flavor number so that the flavor mixing is strongly suppressed.

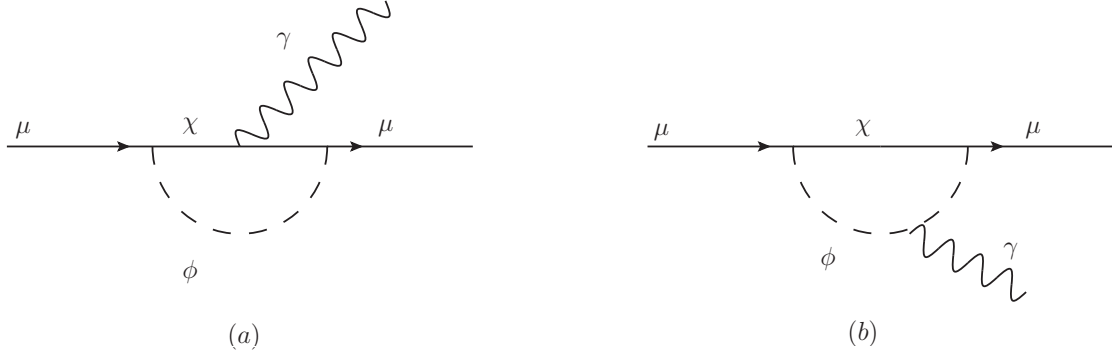


Figure 1: Feynman diagrams for muon $g - 2$

Since the right-handed muon couples to χ and ϕ , their radiative corrections induce the muon $g-2$, a_μ^{new} as shown in Fig. 1. The contribution a_μ^{new} is given by

$$a_\mu^{\text{new}} = -\frac{y_N^2 m_\mu^2}{16\pi^2} [Q_\chi(C_{11} + C_{21})(\phi, \chi, \chi; p, -q) - Q_\phi(C_{12} + C_{22})(\phi, \phi, \chi; q, p - q)], \quad (2.3)$$

where p and $p - q$ are momenta of external muons and q is a photon momentum and a limit $q^2 \rightarrow 0$ is taken. Here $C_X(A, B, C; p_1, p_2)$ ($X = 11, 21, 12, 22$) are so called Passarino-Veltman functions [9], and their definitions in this paper are shown in Appendix. The explicit forms are

$$(C_{11} + C_{21})(\phi, \chi, \chi; p, -q) = \frac{1}{m_\phi^2} \frac{2 - 3y - 6y^2 + y^3 + 6y \log y}{6(1 - y)^4}, \quad (2.4)$$

$$(C_{12} + C_{22})(\phi, \phi, \chi; q, p - q) = \frac{1}{m_\phi^2} \frac{1 - 6y + 3y^2 + 2y^3 - 6y^2 \log y}{6(1 - y)^4}, \quad (2.5)$$

where $y = m_\chi^2/m_\phi^2$, $q^2 = 0$ and the higher order terms of $O(m_\mu^2/m_\phi^2)$ are neglected. The first term in Eq. (2.3) comes from Fig. 1(a) and the second is from Fig. 1(b).

In Fig. 2, we show the contribution to a_μ^{new} as a function of Q_χ and m_ϕ . Here we take $y_N = 2.5$ and $m_\chi = 200$ GeV. We show contours for $(a_\mu^{\text{new}}/10^{-10}) = 2.1, 10.1, 18.1, 26.1, 34.1, 42.1$ and 50.1 , from right to left, corresponding to $-3\sigma, -2\sigma, -1\sigma, 0\sigma, 1\sigma, 2\sigma$ and 3σ deviation from the measured value, respectively. We note that y_N dependence of a_μ^{new} is trivial, that is, a_μ^{new} is proportional to y_N^2 , as shown in Eq. (2.3). For example, if one takes $y_N = 1$, the values of a_μ^{new} in Fig. 2 reduce by a factor $(1/2.5)^2 = 0.16$.

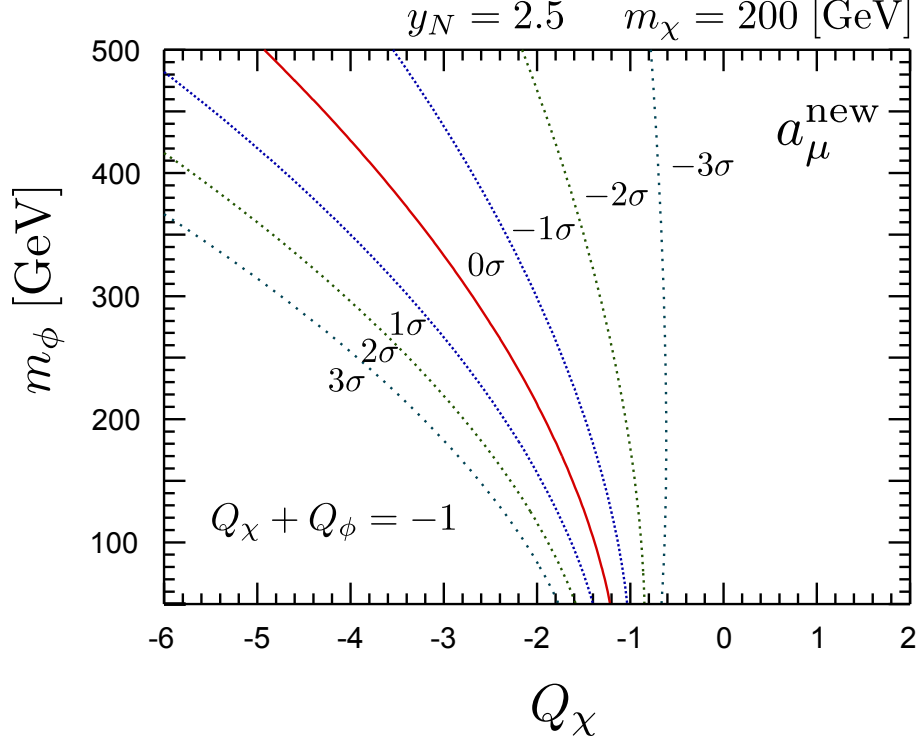


Figure 2: New physics contribution to muon g-2 (a_μ^{new}) as a function of Q_χ and m_ϕ . Here we take $y_N = 2.5$ and $m_\chi = 200$ GeV. We show contours for $(a_\mu^{\text{new}}/10^{-10}) = 2.1, 10.1, 18.1, 26.1, 34.1, 42.1$ and 50.1 , from right to left, corresponding to $-3\sigma, -2\sigma, -1\sigma, 0\sigma, 1\sigma, 2\sigma$ and 3σ deviation from the measured value, respectively.

One can see that the region with $Q_\chi > -1$ (which corresponds to $Q_\phi < 0$) is disfavored by the data of muon g-2. It is interesting to notice that the neutral fermion ($Q_\chi = 0$, corresponding to $Q_\phi = -1$) is difficult to explain the anomaly in any values of m_ϕ , and on the other hand, the neutral scalar ($Q_\phi = 0$, corresponding to $Q_\chi = -1$) can potentially accommodate the anomaly if the scalar ϕ is not so heavy. It is also interesting to note that the multi-charged fermion and scalar (such as $Q_\chi = -2, -3, \dots$, corresponding to $Q_\phi = 1, 2, \dots$) are also favored by the muon g-2 anomaly if m_ϕ is a right value for the anomaly. Therefore, the anomaly of muon g-2 constrains the QED charges as well as the mass scale of new particles.

In Fig. 3, we show a_μ^{new} as a function of m_χ and m_ϕ for (a) $Q_\chi = -1$ (corresponding to $Q_\phi = 0$) and $y_N = 2.5$ and (b) $Q_\chi = -5$ (corresponding to $Q_\phi = 4$) and $y_N = 1.5$. Contours for $(a_\mu^{\text{new}}/10^{-10}) = 2.1, 10.1, 18.1, 26.1, 34.1, 42.1$ and 50.1 (corresponding to $-3\sigma, -2\sigma, -1\sigma, 0\sigma, 1\sigma, 2\sigma$ and 3σ deviation from the measured value) are shown, similar to Fig. 2.^{#2} As one can see, new particles with their masses of about 100 GeV and the coupling $y_N \sim O(1)$

^{#2} If one changes the value of Yukawa coupling y_N , one should simply multiply the value of a_μ^{new} in Fig. 3 (a) and (b) by a factor $(\frac{y_N}{2.5})^2$ and $(\frac{y_N}{1.5})^2$, respectively.

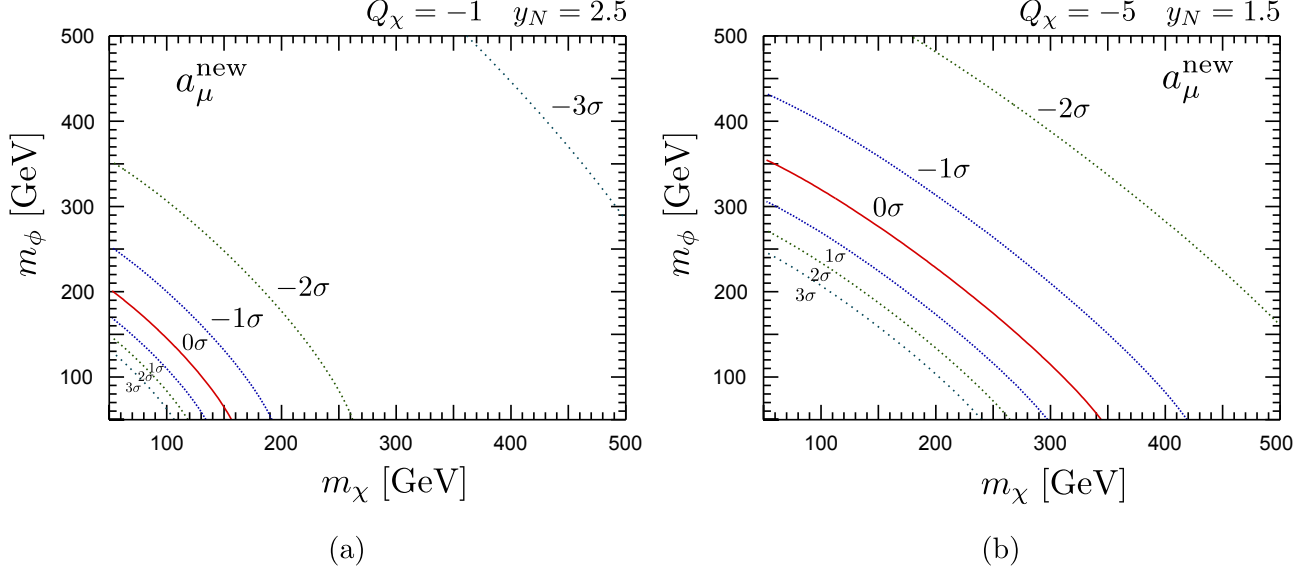


Figure 3: New physics contribution to muon $g-2$ (a_μ^{new}) as a function of m_χ and m_ϕ for (a) $Q_\chi = -1$ and $y_N = 2.5$ (b) $Q_\chi = -5$ and $y_N = 1.5$, respectively. Contours for $(a_\mu^{\text{new}}/10^{-10}) = 2.1, 10.1, 18.1, 26.1, 34.1, 42.1$ and 50.1 (corresponding to $-3\sigma, -2\sigma, -1\sigma, 0\sigma, 1\sigma, 2\sigma$ and 3σ deviation from the measured value) are shown, similar to Fig. 2.

are strongly favored by the anomaly of muon $g-2$ when $Q_\chi = -1$. When the QED charge of χ decreases further negatively (from -1 to -5), the muon $g-2$ gets larger even if the Yukawa coupling y_N gets smaller, as shown in Fig. 3 (b).

Since the anomaly of muon $g-2$ requires relatively light new particles ($\sim O(100 \text{ GeV})$) and/or relatively large Yukawa coupling ($\sim O(1)$) in this scenario, the EW precision observables can be affected by these new particles and new interactions. Therefore, we will check the effects of these particles on the EW observables in a next section.

We would also like to point out that the anomaly of muon $g-2$ suggests the existence of relatively light new particles and/or multi-charged particles. Therefore, it is very interesting to know whether these particles can be found directly or indirectly at the LHC. We will study the direct productions of these particles and the effects on Higgs decay to $\gamma\gamma$ at the LHC in a later section.

2.2 Model where both right- and left-handed muons have new Yukawa couplings

Unlike the previous case, here we consider that both right- and left-handed muons have new Yukawa interactions:

$$\mathcal{L} = -y_L \bar{L}_2 \Phi \chi_R - y_R \bar{\mu}_R \phi \chi_L - m_\chi \bar{\chi}_L \chi_R + \text{h.c.}, \quad (2.6)$$

where $L_2 (= (\nu_{\mu L}, \mu_L)^T)$, $\Phi (= (\phi_1, \phi_2)^T)$ and ϕ are the second generation SU(2) doublet lepton, SU(2) doublet and singlet scalars, respectively, and χ is SU(2) singlet fermion, whose mass is m_χ . Here we have assumed the Z_2 parity again in order to simplify the model. Under the Z_2 parity, the SM particles are even, and new particles ϕ , Φ and χ are odd. We also implicitly assume the approximate muon flavor symmetry, under which χ or (ϕ, Φ) has muon flavor number, so that the flavor mixing of this type of new Yukawa couplings are strongly suppressed. The model we discuss in this paper may be a part of the complete model. However, we think this part of the complete model is crucial for the muon g-2.^{#3}

The QED charges of new particles are represented in term of QED charge of χ field (Q_χ) as follows:

$$Q(\phi_1) \equiv Q_1 = -Q_\chi, \quad (2.7)$$

$$Q(\phi_2) \equiv Q_2 = -1 - Q_\chi, \quad (2.8)$$

$$Q_\phi = -1 - Q_\chi = Q_2. \quad (2.9)$$

Since $Q_\phi = Q_2$, ϕ and ϕ_2 can mix each other. For example, the following gauge invariant term induces the $\phi_2 - \phi$ mixing mass terms after the electroweak symmetry is spontaneously broken:

$$\mathcal{L} = -\lambda M(H^\dagger \Phi \phi^\dagger) + \text{h.c.} = -\frac{\lambda M v}{\sqrt{2}} \phi_2 \phi^\dagger + \dots, \quad (2.10)$$

Here we parameterize the mass terms for ϕ and ϕ_2 as follows: ^{#4}

$$\mathcal{L} = -\begin{pmatrix} \phi^\dagger & \phi_2^\dagger \end{pmatrix} \begin{pmatrix} m_{11}^2 & m_{12}^2 \\ m_{12}^2 & m_{22}^2 \end{pmatrix} \begin{pmatrix} \phi \\ \phi_2 \end{pmatrix}. \quad (2.11)$$

Thus diagonalizing this mass matrix, we define the mass eigenstates s_i ($i = 1, 2$) as

$$\begin{pmatrix} \phi \\ \phi_2 \end{pmatrix}_i = V_{ij} s_j. \quad (2.12)$$

Here V_{ij} is a mixing unitary matrix, which diagonalizes the mass matrix shown in Eq. (2.11). The mass eigen values are taken to be $m_{s_1} < m_{s_2}$. This type of mixing terms are important

^{#3}In summary, we briefly comment on the possible completions of this type of model.

^{#4}When $Q_\phi = 0$, mass term such as $-m^2 \phi \phi_2$ is also possible. Here we neglect such a mass term for simplicity. Even if we include such a mass term, our result does not change qualitatively.

to induce large contribution to muon g-2. The contributions to muon g-2 are summarized by

$$\begin{aligned}
a_\mu^{\text{new}} = & -\frac{Q_\chi m_\mu^2}{16\pi^2} \sum_i \left\{ (y_L^2 |V_{2i}|^2 + y_R^2 |V_{1i}|^2) (C_{11} + C_{21})(s_i, \chi, \chi; p, -q) \right. \\
& \left. + 2y_L y_R \frac{m_\chi}{m_\mu} \text{Re}(V_{2i} V_{1i}^*) C_{11}(s_i, \chi, \chi; p, -q) \right\} \\
& + \frac{Q_2 m_\mu^2}{16\pi^2} \sum_i \left\{ (y_L^2 |V_{2i}|^2 + y_R^2 |V_{1i}|^2) (C_{12} + C_{22})(s_i, s_i, \chi; q, p - q) \right. \\
& \left. + 2y_L y_R \frac{m_\chi}{m_\mu} \text{Re}(V_{2i} V_{1i}^*) C_{12}(s_i, s_i, \chi; q, p - q) \right\}, \quad (2.13)
\end{aligned}$$

where p and $p - q$ are momenta of external muons, and q is a photon momentum and a limit $q^2 \rightarrow 0$ is taken. Here we show the explicit expressions of above Passarino-Veltman functions:

$$(C_{11} + C_{21})(s_i, \chi, \chi; p, -q) = \frac{1}{m_{s_i}^2} \frac{2 + 3y_i - 6y_i^2 + y_i^3 + 6y_i \ln y_i}{6(1 - y_i)^4}, \quad (2.14)$$

$$C_{11}(s_i, \chi, \chi; p, -q) = -\frac{1}{m_{s_i}^2} \frac{3 - 4y_i + y_i^2 + 2 \ln y_i}{2(1 - y_i)^3}, \quad (2.15)$$

$$(C_{22} + C_{12})(s_i, s_i, \chi; q, p - q) = \frac{1}{m_{s_i}^2} \frac{1 - 6y_i + 3y_i^2 + 2y_i^3 - 6y_i^2 \ln y_i}{6(1 - y_i)^4}, \quad (2.16)$$

$$C_{12}(s_i, s_i, \chi; q, p - q) = \frac{1}{m_{s_i}^2} \frac{1 - y_i^2 + 2y_i \ln y_i}{2(1 - y_i)^3}, \quad (2.17)$$

where $y_i = m_\chi^2/m_{s_i}^2$ and we neglected the higher order of $O(m_\mu^2/m_{s_i}^2)$.

The effective operator which expresses the muon g-2 is written by

$$\mathcal{L} = \frac{v}{\Lambda^2} \mu_R \sigma^{\mu\nu} \mu_L F_{\mu\nu} + \text{h.c.}, \quad (2.18)$$

where v is a vacuum expectation value of Higgs boson, and $F_{\mu\nu}$ is a field strength of photon field, and Λ is a typical scale related to new physics. As one see, the chirality of muon has to flip in this interaction. In the case where only right-handed muon has the new Yukawa interaction, the chirality flipping of muon happens in the external muon line in the loop diagram. On the other hands, in the present case where both right- and left-handed muons have the new Yukawa interactions, the chirality flipping can occur in the internal fermion line, which is proportional to the mass of the fermion χ . That is why there are terms which are proportional to $y_R y_L m_\chi/m_\mu$ in Eq. (2.13). This contribution enhances the effects of muon g-2. Therefore, it is very important to explain the anomaly of muon g-2.

In Fig. 4, we show a_μ^{new} as a function of m_χ and m_{s_1} (which is a mass of lighter scalar state) in case of (a) $Q_\chi = -1$ and (b) $Q_\chi = 0$. Contours for $(a_\mu^{\text{new}}/10^{-10}) = 2.1, 10.1, 18.1, 26.1, 34.1, 42.1$ and 50.1 (corresponding to $-3\sigma, -2\sigma, -1\sigma, 0\sigma, 1\sigma, 2\sigma$ and 3σ deviation from the measured value) are shown. Here we took $m_{11}^2 = m_{22}^2, m_{12}^2 = (50 \text{ GeV})^2$,

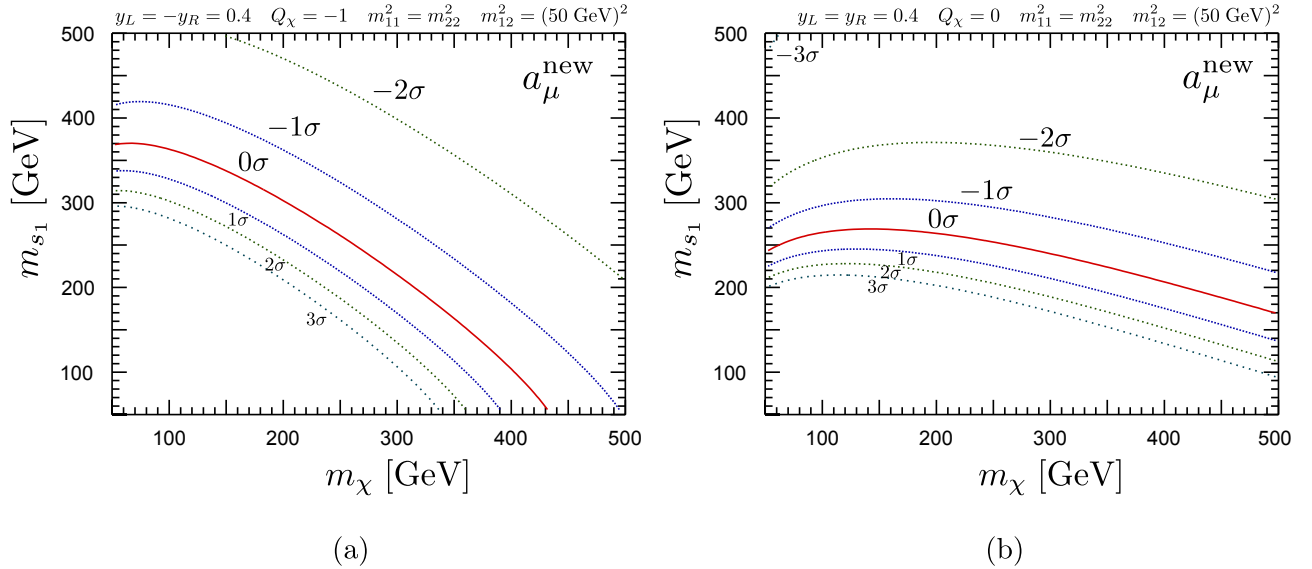


Figure 4: New physics contribution to muon g-2 (a_μ^{new}) as a function of m_χ and m_{s_1} in case of (a) $Q_\chi = -1$ and (b) $Q_\chi = 0$. Contours for $(a_\mu^{\text{new}}/10^{-10}) = 2.1, 10.1, 18.1, 26.1, 34.1, 42.1$ and 50.1 (corresponding to $-3\sigma, -2\sigma, -1\sigma, 0\sigma, 1\sigma, 2\sigma$ and 3σ deviation from the measured value) are shown. Here we assume that $m_{11}^2 = m_{22}^2, m_{12}^2 = (50 \text{ GeV})^2$. We also take (a) $y_L = -y_R = 0.4$ and (b) $y_L = y_R = 0.4$.

and (a) $y_L = -y_R = 0.4$ (b) $y_L = y_R = 0.4$. Note that in order to generate the positive contribution to muon g-2 in Fig. 4 (a), the sign of new Yukawa couplings had to be taken as $y_L y_R < 0$. On the other hand, in Fig. 4 (b), the sign of $y_L y_R$ should be positive. As shown in Fig. 4, compared to Fig. 3, even smaller Yukawa couplings and heavier new particles can accommodate the anomaly of muon g-2 because of the enhancement mentioned above. As can be seen from Fig. 4, when $y_L \sim y_R \sim O(1)$, the EW scale new particles are expected in order to explain the anomaly of muon g-2. Therefore, we will analyze the effects on the EW precision observables and show the consistent region of parameters in a next section.

3 Effects on electroweak observables

In the previous section, we showed that the relatively light new particles are required in order to explain the anomaly of muon g-2. In addition, in the case where the only right-handed muon has new Yukawa interaction, the new Yukawa coupling should be relatively large for the anomaly of muon g-2. Therefore, we should check if the relatively light particles and the relatively large Yukawa coupling are consistent with the EW precision measurements. Although models which we consider in this paper may be only a part of complete models, we should know how these new particles affect EW observables.

In this section, we adopt the formalism in Refs.[10, 11, 12] in order to include the oblique

corrections as well as the vertex corrections in the EW observables. First we briefly summarize the formalism [10, 11, 12].

In the presence of EW to TeV scale physics, it is well known that the oblique corrections in gauge boson self-energy are important. They are parameterized by Peskin-Takeuchi's S, T, U parameters [13, 14, 15]:

$$\frac{\alpha S}{4s_W^2 c_W^2} = \frac{\Pi_{ZZ}(M_Z^2) - \Pi_{ZZ}(0)}{M_Z^2} - \frac{c_{2W}}{c_W s_W} \frac{\Pi_{Z\gamma}(M_Z^2)}{M_Z^2} - \frac{\Pi_{\gamma\gamma}(M_Z^2)}{M_Z^2}, \quad (3.19)$$

$$\alpha T = \frac{\Pi_{WW}(0)}{M_W^2} - \frac{\Pi_{ZZ}(0)}{M_Z^2}, \quad (3.20)$$

$$\begin{aligned} \frac{\alpha U}{4s_W^2} &= \frac{\Pi_{WW}(M_W^2) - \Pi_{WW}(0)}{M_W^2} - c_W^2 \frac{\Pi_{ZZ}(M_Z^2) - \Pi_{ZZ}(0)}{M_Z^2} \\ &\quad - 2s_W c_W \frac{\Pi_{Z\gamma}(M_Z^2)}{M_Z^2} - s_W^2 \frac{\Pi_{\gamma\gamma}(M_Z^2)}{M_Z^2}. \end{aligned} \quad (3.21)$$

Here we use the notation c_W and s_W to refer to the cosine and sine of the weak mixing angle and $c_{2W} = c_W^2 - s_W^2$. In addition, in Refs.[10, 11], R_Z and R_W parameters are introduced in order to account for the smaller corrections:

$$\frac{\alpha R_Z}{4s_W^2 c_W^2} = \left. \frac{d\Pi_{ZZ}(p^2)}{dp^2} \right|_{p^2=M_Z^2} - \frac{\Pi_{ZZ}(M_Z^2) - \Pi_{ZZ}(0)}{M_Z^2}, \quad (3.22)$$

$$\frac{\alpha R_W}{4s_W^2} = \frac{\Pi_{WW}(M_Z^2) - \Pi_{WW}(M_W^2)}{M_Z^2 - M_W^2} - \frac{\Pi_{WW}(M_W^2) - \Pi_{WW}(0)}{M_W^2}. \quad (3.23)$$

Furthermore, new particles have effects on the running QED coupling constant $\alpha(M_Z^2)$ [3, 12]:

$$\alpha(M_Z^2) = \frac{\alpha}{1 - \Delta\alpha_{\text{lep}}(M_Z^2) - \Delta\alpha_{\text{had}}^{(5)}(M_Z^2) - \Delta\alpha_{\text{top}}(M_Z^2) - \Delta\alpha_{\text{new}}(M_Z^2)} \quad (3.24)$$

Here $\Delta\alpha_{\text{lep}}(M_Z^2)$, $\Delta\alpha_{\text{had}}^{(5)}(M_Z^2)$, $\Delta\alpha_{\text{top}}(M_Z^2)$, and $\Delta\alpha_{\text{new}}(M_Z^2)$ are the leptonic, the five-flavor hadronic, the top quark and the new physics contributions to the running of the QED coupling constant respectively. The new physics contributions to the running of the QED coupling constant $\Delta\alpha_{\text{new}}(M_Z^2)$ are defined as

$$\Delta\alpha_{\text{new}}(M_Z^2) = \frac{\Pi_{\gamma\gamma}(M_Z^2)}{M_Z^2} - \left. \frac{\Pi_{\gamma\gamma}(p^2)}{p^2} \right|_{p^2=0} \quad (3.25)$$

These oblique parameters contribute to EW observables, as shown in Refs. [10, 11, 12].

If muon has $O(1)$ new Yukawa couplings,^{#5} it induces non-universal vertex corrections to the $Z\mu^+\mu^-$ coupling. The standard model coupling of $Z\mu^+\mu^-$ is given by

$$i \frac{g}{c_W} \gamma_\mu [g_L^{\text{SM},\mu} P_L + g_R^{\text{SM},\mu} P_R], \quad (3.26)$$

^{#5}In this paper, we assume that electron and tau do not have $O(1)$ extra Yukawa couplings, for simplicity.

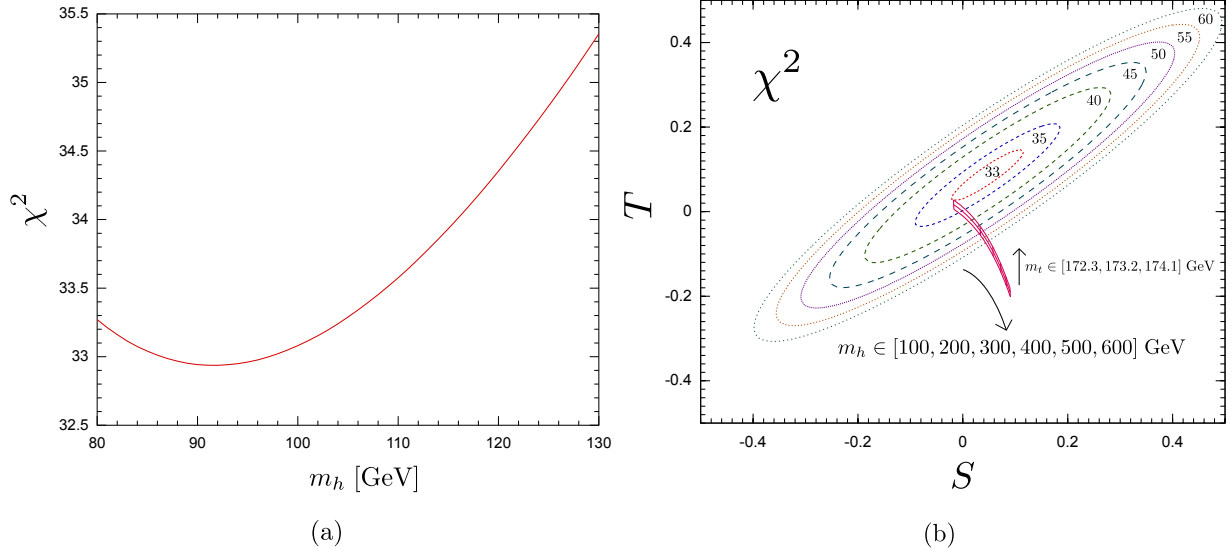


Figure 5: (a) χ^2 of the EW observables listed in Table. 1 as a function of the Higgs boson mass m_h within the SM. (b) χ^2 contours shown in dashed lines in S-T plane, assuming that other oblique corrections (U , R_W , R_Z) and vertex corrections are zero. Reference Higgs boson mass and top quark mass are taken to be 125 GeV and 173.2 GeV, respectively. We also show the predicted S-T values (shown in solid lines) in the SM, varying the Higgs boson mass and top quark mass from the reference values.

where $g_{L,R}^{\text{SM},\mu}$ are the standard model couplings, and their tree level contributions are $g_L^{\text{SM},\mu} = -\frac{1}{2} + s_W^2$ and $g_R^{\text{SM},\mu} = s_W^2$. When we take into account of corrections to $Z\mu^+\mu^-$ vertex via the new Yukawa coupling (including the corresponding wave function renormalization), the $Z\mu^+\mu^-$ coupling is modified by

$$i\frac{g}{c_W}\gamma_\mu \left[(g_L^{\text{SM},\mu} + \Delta g_L^\mu)P_L + (g_R^{\text{SM},\mu} + \Delta g_R^\mu)P_R \right]. \quad (3.27)$$

Here the vertex corrections generated by new particles are parameterized by $\Delta g_{L,R}^\mu$.

The corrections to $W\mu\nu_\mu$ vertex generates the corrections to the Fermi constant G_F and therefore, we parameterize it as $\Delta\bar{\delta}_G$. The $\Delta\bar{\delta}_G$ for the new physics contributions from the vertex and box diagrams to the μ -decay process is defined as

$$G_F = G_F^{\text{SM+ob.}} + \frac{g^2}{4\sqrt{2}M_W^2}\Delta\bar{\delta}_G. \quad (3.28)$$

Here $G_F^{\text{SM+ob.}}$ is the muon decay constant including effects of SM radiative corrections and new physics oblique corrections except the vertex and box corrections from new physics.

Using the formalism in Ref.[10, 11], one can calculate EW observables listed in Table 1 without assuming lepton universality. First, we show a result of the SM fit of the EW observables in Fig. 5 (a) as a function of Higgs boson mass m_h . The best fit point is at

	data	SM fit	pull	Sample model	pull
line-shape & FB asym.:					
$\Gamma_Z(\text{GeV})$	2.4952(23)	2.4954	-0.1	2.4963	-0.5
$\sigma_h^0(\text{nb})$	41.541(37)	41.479	1.7	41.479	1.7
R_e	20.804(50)	20.740	1.3	20.741	1.3
R_μ	20.785(33)	20.740	1.4	20.740	1.3
R_τ	20.764(45)	20.787	-0.5	20.788	-0.5
$A_{\text{FB}}^{0,e}$	0.0145(25)	0.0163	-0.7	0.0163	-0.7
$A_{\text{FB}}^{0,\mu}$	0.0169(13)	0.0163	0.5	0.0163	0.4
$A_{\text{FB}}^{0,\tau}$	0.0188(17)	0.0163	1.5	0.0163	1.4
τ polarization:					
A_τ	0.1439(43)	0.1472	-0.8	0.1476	-0.9
A_e	0.1498(49)	0.1472	0.5	0.1476	0.4
b and c quark results:					
R_b	0.21629(66)	0.21579	0.8	0.21580	0.7
R_c	0.1721(30)	0.1723	-0.1	0.1722	0.0
$A_{\text{FB}}^{0,b}$	0.0992(16)	0.1032	-2.5	0.1035	-2.7
$A_{\text{FB}}^{0,c}$	0.0707(35)	0.0738	-0.9	0.0740	-0.9
A_b	0.923(20)	0.935	-0.6	0.935	-0.6
A_c	0.670(27)	0.668	0.1	0.668	0.1
SLD results:					
A_e	0.1516(21)	0.1472	2.1	0.1476	1.9
A_μ	0.142(15)	0.1472	-0.4	0.1476	-0.4
A_τ	0.136(15)	0.1472	-0.8	0.1476	-0.8
W mass and width:					
$M_W(\text{GeV})$	80.385(15)[16]	80.363	1.5	80.376	0.6
$\Gamma_W(\text{GeV})$	2.085(42)	2.091	-0.1	2.092	-0.2
muon g-2:					
$a_\mu^{\text{new}}(10^{-9})$	2.61(0.80)	0	3.3	3.15	-0.7
Input parameters					
$\Delta\alpha_{\text{had}}^{(5)}(M_Z^2)$	0.027626(138)	0.027592	0.3	0.027626	0.0
$\alpha_s(M_Z)$	0.1184(7)	0.1184	0.0	0.1184	0.0
$m_t(\text{GeV})$	173.2(0.9)[17]	173.7	-0.6	173.3	-0.1
$m_h(\text{GeV})$		125		125	
$y_L = y_R, Q_\chi$	-	-	-	0.4, 0	
$m_{\phi_1}, m_\chi(\text{GeV})$	-	-	-	300, 200	
$m_{11}^2 = m_{22}^2, m_{12}^2(\text{GeV})^2$	-	-	-	(250) ² , (50) ²	
$\chi^2/(d.o.f)$		34.8/(22)		22.5/(15)	

Table 1: Experimental data and theoretical predictions of electroweak observables. The predicted values of the SM and sample model discussed in Sec. 3.2 are shown.

$m_h = 91$ GeV. This is consistent with the result shown by the LEP electroweak working group [18]. In Table 1, we show the SM fit when Higgs boson mass is assumed to be 125 GeV, which has been suggested by the latest LHC data. In Fig. 5(b), χ^2 contours are shown in dashed lines in S-T plane. Here we assume that other oblique corrections (U , R_W , R_Z) and vertex corrections are zero. Reference Higgs boson mass and top quark mass are taken to be 125 GeV, 173.2 GeV, respectively. The predicted values of S-T parameters are also shown by varying the Higgs boson mass and top quark mass from the reference values. We note that the SM fit with lighter Higgs boson is good except for the muon g-2, and small positive S and T ($S \sim 0.05$, $T \sim 0.1$) can decrease the χ^2 further. Therefore, we need new physics which largely contributes to muon g-2, but whose effects on other EW observables are small. In this section, we analyze the EW observables in models discussed in the previous section. In this analysis, we assume $m_h = 125$ GeV.

3.1 Model with SU(2) singlet scalar (ϕ) and singlet Dirac fermion (χ)

Since the new scalar ϕ and new fermion χ are SU(2) singlet, they do not couple to W boson. But if it has a QED charge, it can couple to photon and Z boson. Here we list the corrections to self-energy functions of gauge bosons in this model.

The singlet fermion (χ) contributions are given by

$$\begin{aligned}
\Pi_{WW}^{(\chi)}(p^2) &= 0 \\
\Pi_{ZZ}^{(\chi)}(p^2) &= -\frac{g^2 Q_\chi^2 s_W^4}{4\pi^2 c_W^2} [m_\chi^2 B_0(\chi, \chi) - p^2 \{B_1(\chi, \chi) + B_{21}(\chi, \chi)\} - 2(1 - \epsilon) B_{22}(\chi, \chi)], \\
\Pi_{\gamma\gamma}^{(\chi)}(p^2) &= -\frac{e^2}{4\pi^2} Q_\chi^2 [m_\chi^2 B_0(\chi, \chi) - p^2 \{B_1(\chi, \chi) + B_{21}(\chi, \chi)\} - 2(1 - \epsilon) B_{22}(\chi, \chi)], \\
\Pi_{\gamma Z}^{(\chi)}(p^2) &= \frac{ge Q_\chi^2 s_W^2}{4\pi^2 c_W} [m_\chi^2 B_0(\chi, \chi) - p^2 \{B_1(\chi, \chi) + B_{21}(\chi, \chi)\} - 2(1 - \epsilon) B_{22}(\chi, \chi)].
\end{aligned} \tag{3.29}$$

Here $B_X(i, j) = B_X(m_i^2, m_j^2; p)$ ($X = 0, 1, 21, 22$), which are Passarino-Veltman functions and are shown explicitly in Appendix. We use the dimensional regularization in space-time dimension $D = 4 - 2\epsilon$.

The singlet scalar (ϕ) contributions are given by

$$\begin{aligned}
\Pi_{WW}^{(\phi)}(p^2) &= 0 \\
\Pi_{ZZ}^{(\phi)}(p^2) &= \frac{g^2}{4\pi^2 c_W^2} Q_\phi^2 s_W^4 \left\{ B_{22}(\phi, \phi) - \frac{1}{2} A(\phi) \right\}, \\
\Pi_{\gamma\gamma}^{(\phi)}(p^2) &= \frac{e^2}{4\pi^2} Q_\phi^2 \left\{ B_{22}(\phi, \phi) - \frac{1}{2} A(\phi) \right\}, \\
\Pi_{\gamma Z}^{(\phi)}(p^2) &= -\frac{ge}{4\pi^2 c_W} Q_\phi^2 s_W^2 \left\{ B_{22}(\phi, \phi) - \frac{1}{2} A(\phi) \right\}.
\end{aligned} \tag{3.30}$$

Here Passarino-Veltman functions $B_{22}(i, j)(= B_{22}(m_i^2, m_j^2; p))$ and $A(\phi)$ are shown in Appendix. We can easily show that Peskin-Takeuchi STU parameters in this case vanish ($S = T = U = 0$), since the new particles do not have $SU(2)_L$ interactions. Thus, the leading contributions to the oblique corrections are R_Z parameter and $\Delta\alpha_{\text{new}}(M_Z^2)$:

$$R_Z = \frac{4s_W^4 Q_\chi^2}{3\pi} \left[1 + \frac{6m_\chi^2}{M_Z^2} \left\{ 1 - \frac{\frac{4m_\chi^2}{M_Z^2}}{\sqrt{\frac{4m_\chi^2}{M_Z^2} - 1}} \tan^{-1} \left[\frac{1}{\sqrt{\frac{4m_\chi^2}{M_Z^2} - 1}} \right] \right\} \right] \\ + \frac{s_W^4 Q_\phi^2}{3\pi} \left[1 - \frac{12m_\phi^2}{M_Z^2} \left\{ 1 - \sqrt{\frac{4m_\phi^2}{M_Z^2} - 1} \tan^{-1} \left[\frac{1}{\sqrt{\frac{4m_\phi^2}{M_Z^2} - 1}} \right] \right\} \right], \quad (3.31)$$

$$\Delta\alpha_{\text{new}}(M_Z^2) = -\frac{5\alpha Q_\chi^2}{9\pi} \left[1 + \frac{12m_\chi^2}{5M_Z^2} - \frac{6}{5} \left(1 + \frac{2m_\chi^2}{M_Z^2} \right) \sqrt{\frac{4m_\chi^2}{M_Z^2} - 1} \tan^{-1} \left[\frac{1}{\sqrt{\frac{4m_\chi^2}{M_Z^2} - 1}} \right] \right] \\ - \frac{2\alpha Q_\phi^2}{9\pi} \left[1 - \frac{3m_\phi^2}{M_Z^2} + \frac{3}{4} \sqrt{\frac{4m_\phi^2}{M_Z^2} - 1} \tan^{-1} \left[\frac{1}{\sqrt{\frac{4m_\phi^2}{M_Z^2} - 1}} \right] \right], \quad (3.32)$$

where we assume $2m_\chi > M_Z$ and $2m_\phi > M_Z$.

As discussed in the previous section, in order to explain the anomaly of muon g-2, the new Yukawa coupling in this model should be relatively large. In this case, the potentially large vertex corrections may be expected, as shown in Fig.6. The results are expressed by

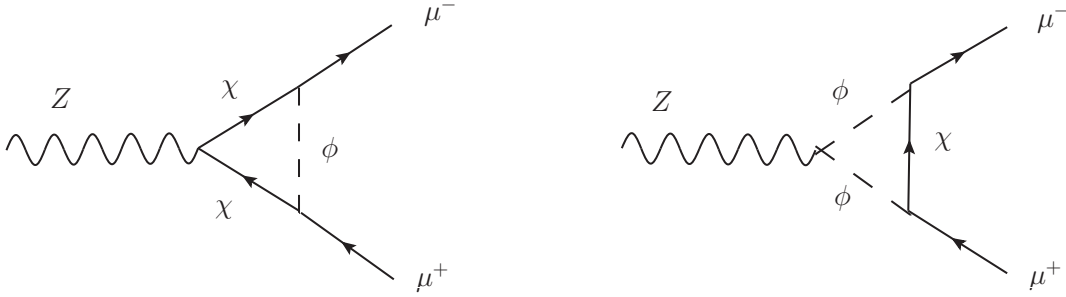


Figure 6: Feynman diagrams for vertex corrections to $Z\mu^+\mu^-$ coupling.

$$\Delta g_L^\mu = 0, \quad (3.33)$$

$$\begin{aligned} \Delta g_R^\mu &= \frac{y_N^2}{16\pi^2} \left[-2Q_\phi s_W^2 C_{24}(\phi, \chi, \phi; p, q-p) \right. \\ &\quad \left. + Q_\chi s_W^2 \left\{ \frac{1}{2} - 2C_{24} - M_Z^2(C_{12} + C_{23}) + m_\chi^2 C_0 \right\} (\chi, \phi, \chi; q-p, p) \right. \\ &\quad \left. - s_W^2 (B_0 + B_1)(\phi, \chi; p) \right], \end{aligned} \quad (3.34)$$

where p , $q-p$ and q are muon, anti-muon and Z-boson momenta, respectively. Here Passarino-Veltman functions C_X ($X = 0, 12, 23, 24$) and B_X ($X = 0, 1$) are explicitly shown in Appendix.

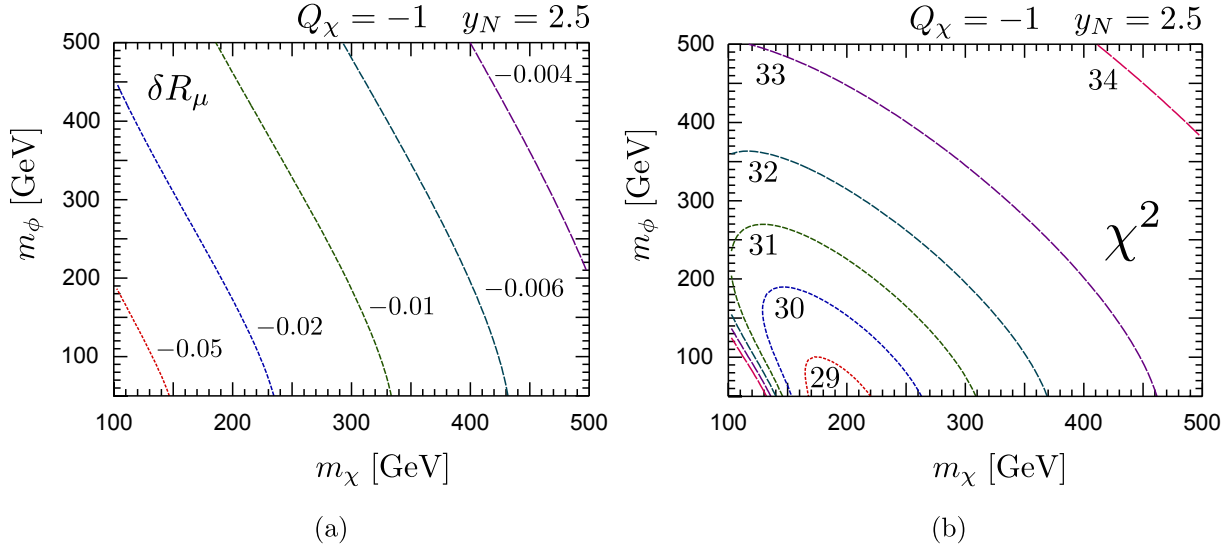


Figure 7: (a) Effect of vertex corrections on R_μ . $\delta R_\mu = R_\mu - R'_\mu$ are shown as a function of m_χ and m_ϕ in case of $Q_\chi = -1$ and $y_N = 2.5$, where R_μ includes all corrections, and R'_μ contains all corrections except for the vertex corrections. (b) χ^2 as a function of m_χ and m_ϕ in case of $Q_\chi = -1$ and $y_N = 2.5$.

The vertex corrections affect EW observables such as R_μ , $A_{\text{FB}}^{0,\mu}$, and A_μ . Among these observables, we find that the effect on the R_μ is the most important in the fit because R_μ is most precisely measured. In Fig.7 (a), we show the effect of vertex corrections in R_μ , that is, $\delta R_\mu = R_\mu - R'_\mu$ as a function of m_χ and m_ϕ in case of $Q_\chi = -1$ and $y_N = 2.5$. Here R_μ is a theoretical prediction in this model containing all corrections, on the other hand, R'_μ contains all corrections except for the vertex corrections. The difference δR_μ shows the effect of the vertex corrections. Note that the size of experimental error of R_μ is 0.033 for 1σ , as shown in Table. 1. As one can see in Fig. 7(a), the vertex correction can change the prediction of R_μ about 1σ in the region where the muon g-2 can be explained by the new physics contributions. Since the SM prediction of R_μ is smaller than that of the experimental

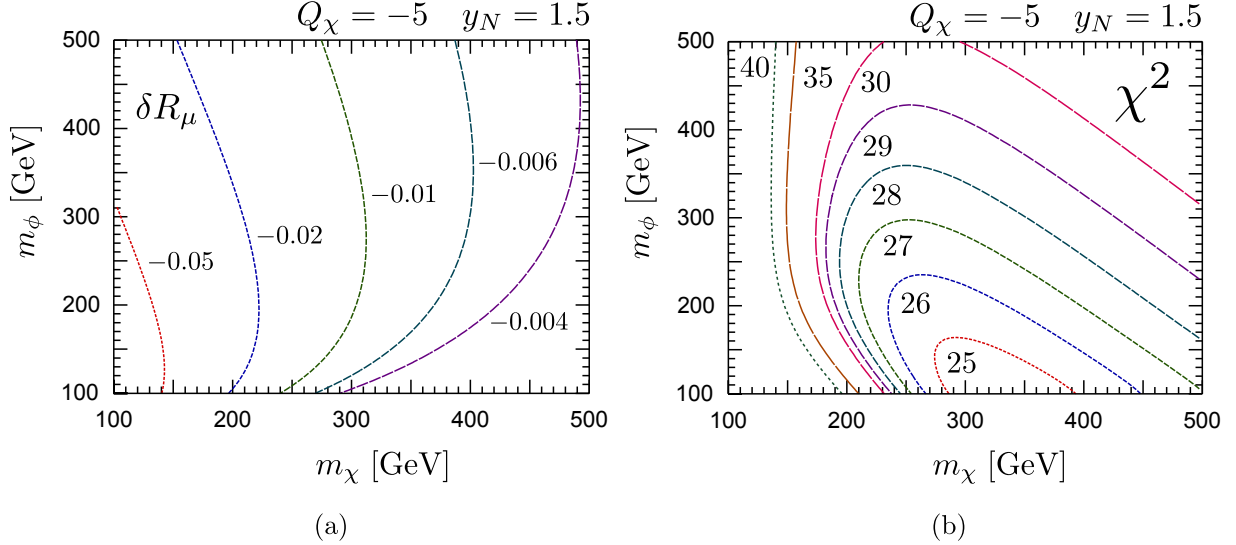


Figure 8: (a) Effect of vertex corrections on R_μ . $\delta R_\mu = R_\mu - R'_\mu$ is shown as a function of m_χ and m_ϕ in case of $Q_\chi = -5$ and $y_N = 1.5$, similar to Fig. 7(a). (b) χ^2 as a function of m_χ and m_ϕ in case of $Q_\chi = -5$ and $y_N = 1.5$.

result (shown in Table. 1), the vertex corrections do not help to improve the prediction of R_μ . Therefore, the region of small χ mass is very constrained.

In Fig. 7 (b), χ^2 is shown as a function of m_χ and m_ϕ in case of $Q_\chi = -1$ and $y_N = 2.5$. As one can see from the figure, χ^2 is large in the region of small m_χ because of the large vertex corrections, discussed above. In the region of larger m_χ and m_ϕ , it is difficult to explain the anomaly of muon g-2 because new particles are too heavy, and hence the χ^2 gets larger. The minimum of χ^2 is around $m_\chi \sim 200$ GeV and $m_\phi \sim 100$ GeV, and we see that the light new particles are favored by the EW observables including muon g-2.

In Fig. 8 (a), the effect of vertex corrections on R_μ , δR_μ is shown in case of $Q_\chi = -5$ and $y_N = 1.5$, similar to Fig. 7 (a). The vertex corrections can be as large as 1σ of the experimental error of R_μ , and they increase the χ^2 . In Fig. 8 (b), the χ^2 is shown as a function of m_χ and m_ϕ . As one can see, the region of small m_χ is disfavored by the vertex corrections of R_μ , as shown in Fig. 8 (a). The minimum of the χ^2 is around $m_\chi \sim 300$ GeV and $m_\phi \sim 100$ GeV. Therefore, the EW precision measurements (including muon g-2) prefer the relatively light new particles in this case.

3.2 Model with SU(2) doublet (Φ) and singlet (ϕ) scalar, and singlet fermion (χ)

The singlet fermion contributions are same as those in the previous case. Here, we list the one loop contributions to gauge boson self-energies induced by scalar sectors.

$$\Pi_{WW}^{(s)}(p^2) = \frac{g^2}{8\pi^2} \left[\sum_i \left\{ |V_{2i}|^2 B_{22}(\phi_1, s_i) - \frac{1}{4} |V_{2i}|^2 A(s_i) \right\} - \frac{1}{4} A(\phi_1) \right], \quad (3.35)$$

$$\begin{aligned} \Pi_{ZZ}^{(s)}(p^2) = & \frac{1}{4\pi} \frac{g^2}{c_W^2} \left[\left(\frac{1}{2} - Q_1 s_W^2 \right)^2 \left\{ B_{22}(\phi_1, \phi_1) - \frac{1}{2} A(\phi_1) \right\} \right. \\ & + \sum_{ij} \left\{ \left(-\frac{1}{2} - Q_2 s_W^2 \right)^2 |V_{2i}|^2 |V_{2j}|^2 + Q_2^2 s_W^4 |V_{1i}|^2 |V_{1j}|^2 \right. \\ & - Q_2 s_W^2 \left(-\frac{1}{2} - Q_2 s_W^2 \right) (V_{2i}^* V_{1i} V_{1j}^* V_{2j} + V_{2j}^* V_{1j} V_{1i}^* V_{2i}) \left. \right\} B_{22}(s_i, s_j) \\ & \left. - \sum_i \left\{ \left(-\frac{1}{2} - Q_2 s_W^2 \right)^2 |V_{2i}|^2 + Q_2^2 s_W^4 |V_{1i}|^2 \right\} \frac{1}{2} A(s_i) \right], \quad (3.36) \end{aligned}$$

$$\begin{aligned} \Pi_{\gamma\gamma}^{(s)}(p^2) = & \frac{e^2}{4\pi^2} \left[Q_1^2 \left\{ B_{22}(\phi_1, \phi_1) - \frac{1}{2} A(\phi_1) \right\} \right. \\ & \left. + Q_2^2 \sum_i \left\{ B_{22}(s_i, s_i) - \frac{1}{2} A(s_i) \right\} \right], \quad (3.37) \end{aligned}$$

$$\begin{aligned} \Pi_{\gamma Z}^{(s)}(p^2) = & \frac{e}{4\pi^2} \frac{g}{c_W} \left[Q_1 \left(\frac{1}{2} - Q_1 s_W^2 \right) \left\{ B_{22}(\phi_1, \phi_1) - \frac{1}{2} A(\phi_1) \right\} \right. \\ & + Q_2 \sum_i \left\{ \left(-\frac{1}{2} - Q_2 s_W^2 \right) |V_{2i}|^2 - Q_2 s_W^2 |V_{1i}|^2 \right\} \\ & \left. \times \left\{ B_{22}(s_i, s_i) - \frac{1}{2} A(s_i) \right\} \right], \quad (3.38) \end{aligned}$$

where Passarino-Veltman functions $B_X(i, j)(= B_X(m_i^2, m_j^2; p))$ and $A(i)$ are shown in Appendix. Unlike the previous model, SU(2) scalar doublet can contribute to the STU parameters. Therefore, the dominant quantum corrections are represented by S and T parameters. To understand a behavior of S and T parameters, here we show the approximate expression of S and T parameters,

$$\begin{aligned} S & \simeq \frac{Y_\Phi}{6\pi} \Delta + \dots, \\ T & \simeq \frac{m_{\phi_1}^2}{16\pi s_W^2 M_W^2} (\Delta)^2 + \dots. \end{aligned} \quad (3.39)$$

Here, for simplicity, we assume that $V_{22} = V_{11} = 1$, $V_{12} = V_{21} = 0$ so that s_2 state originates from ϕ_2 component of SU(2) scalar doublet Φ , and $\Delta = (m_{\phi_2}^2 - m_{\phi_1}^2)/m_{\phi_1}^2$ where $m_{\phi_2} = m_{s_2}$ in this case. Here we ignore the higher order terms of Δ and $m_Z^2/m_{\phi_1}^2$ in Eqs. (3.39). Note that Δ parameterizes non-degeneracy in the SU(2) scalar doublet Φ . Y_Φ is a hypercharge of Φ , $Y_\Phi = \frac{1}{2} + Q_2$. We note that the non-degeneracy of SU(2) scalar doublet generates non-zero T and non-zero S, and T is always positive, but S can be positive or negative depending on signs of Y_Φ and Δ in this model.

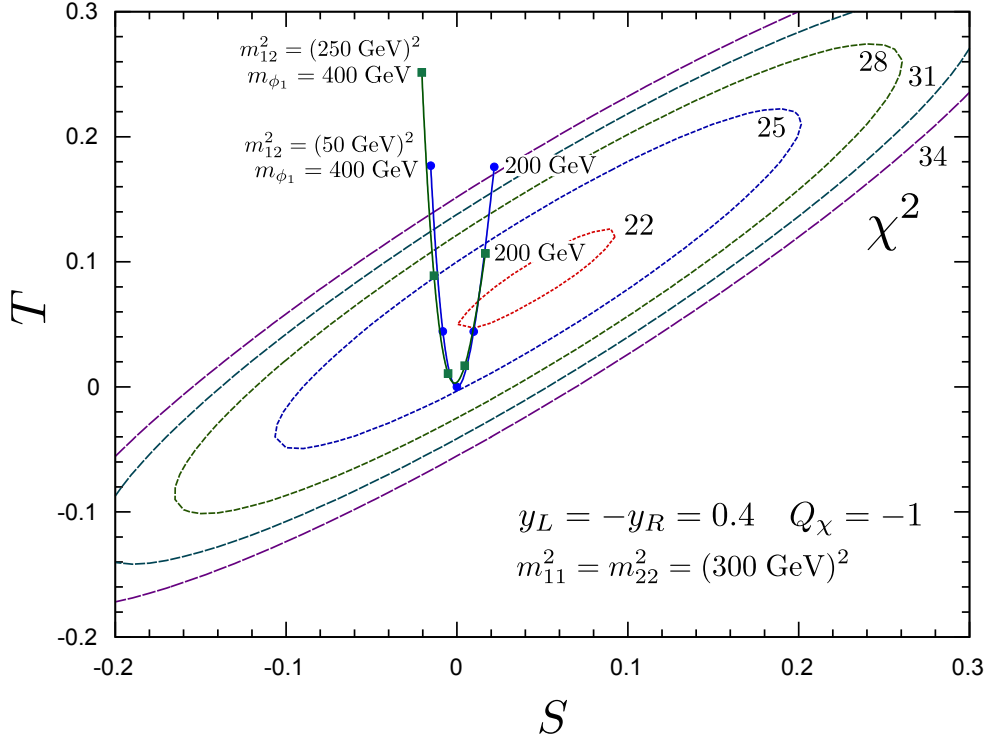


Figure 9: χ^2 contours (without including muon g-2 result) in S-T plane ($\chi^2 = 22$ to 34 in dashed lines) and S-T values (solid lines with points) in this model. Here we take $y_L = -y_R = 0.4$, $Q_\chi = -1$ (corresponding to $Q_1 = 1$ and $Q_2 = 0$), and $m_{11}^2 = m_{22}^2 = (300 \text{ GeV})^2$. Two solid lines correspond to two different values of m_{12}^2 , $m_{12}^2 = (50 \text{ GeV})^2$ and $(250 \text{ GeV})^2$, varying m_{ϕ_1} from 200 GeV to 400 GeV at 50 GeV step.

In Fig. 9, we show numerical result of χ^2 contours in S-T plane (without including muon g-2 result), shown in dashed lines. To draw the χ^2 contours in S-T plane, we assume that other oblique corrections (U , R_Z , and R_W) and vertex corrections are zero. As one can see from the figure, slightly positive S and T ($S \sim 0.05$ and $T \sim 0.1$) are favored by EW observables. In Fig. 9, we also show the predicted values of S-T parameters in this model, shown in solid lines. Here we took $y_L = -y_R = 0.4$, $Q_\chi = -1$ (corresponding to $Q_1 = 1$ and $Q_2 = 0$), and $m_{11}^2 = m_{22}^2 = (300 \text{ GeV})^2$. Two solid lines correspond to two different values of m_{12}^2 , $m_{12}^2 = (50 \text{ GeV})^2$ and $(250 \text{ GeV})^2$. The points on the solid lines represent the predicted

values of S and T , varying m_{ϕ_1} from 200 GeV to 400 GeV at 50 GeV step.

When $m_{11}^2 = m_{22}^2 = (300 \text{ GeV})^2$ and $m_{12}^2 = (50 \text{ GeV})^2$, $m_{s_1} \simeq 296 \text{ GeV}$ and $m_{s_2} \simeq 304 \text{ GeV}$. As roughly shown in Eqs. (3.39), when $m_{\phi_1} = 200 \text{ GeV}$ and $Q_2 = 0$, $\Delta > 0$ and $Y_\Phi = \frac{1}{2} > 0$, and hence $S > 0$ and $T > 0$. As m_{ϕ_1} becomes larger and about 300 GeV, both S and T get closer to zero because the doublet scalars are almost degenerate. Then when m_{ϕ_1} is increased further, S gets negative because $\Delta < 0$, but $T > 0$. In Fig. 9, one can see this behavior. Even when we increase m_{12}^2 , we can see that this behavior is almost same.

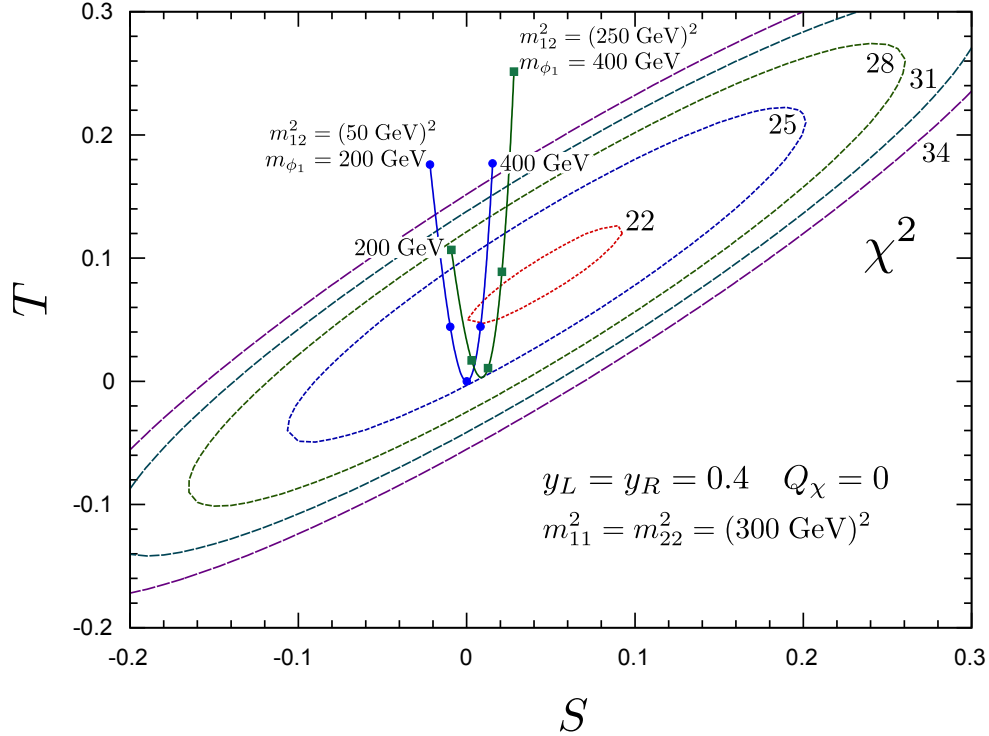


Figure 10: Same as Fig. 9 except for $y_L = y_R = 0.4$ and $Q_\chi = 0$ (corresponding to $Q_1 = 0$ and $Q_2 = -1$).

In Fig. 10, the same figure is shown except for $y_L = y_R = 0.4$ and $Q_\chi = 0$ (corresponding to $Q_1 = 0$ and $Q_2 = -1$). When $Q_\chi = 0$ ($Q_2 = -1$) and $m_{\phi_1} = 200 \text{ GeV}$, $Y_\Phi = -\frac{1}{2} < 0$ and $\Delta > 0$, so that S is negative. As m_{ϕ_1} gets larger, S gets larger. For $m_{\phi_1} \sim 300 \text{ GeV}$, $S \sim 0$ because the doublet scalars are almost degenerate. For $m_{\phi_1} > 300 \text{ GeV}$, S becomes positive. This behavior is different from the previous case with $Q_2 = 0$ since the sign of Y_Φ is different. Note that T is always positive unless SU(2) scalar doublet is degenerate. As one can see in both cases, the small non-degeneracy of SU(2) scalar doublet can make χ^2 better.

In our numerical analysis, we also include the vertex corrections in $Z\mu^+\mu^-$, $Z\nu_\mu\bar{\nu}_\mu$ and $W\mu\nu_\mu$ vertices even though the Yukawa couplings y_L and y_R can be small in this model. The

expression of the vertex corrections is summarized as follows:

$$\begin{aligned}\Delta g_L^\mu &= \frac{y_L^2}{16\pi^2} \left[2 \sum_{ij} \left\{ \left(-\frac{1}{2} - Q_\phi s_W^2 \right) V_{2i}^* V_{2j} - Q_\phi s_W^2 V_{1i}^* V_{1j} \right\} V_{2i} V_{2j}^* C_{24}(s_i, \chi, s_j; p, q - p) \right. \\ &\quad + \sum_i Q_\chi s_W^2 |V_{2i}|^2 \left\{ \frac{1}{2} - 2C_{24} - M_Z^2(C_{12} + C_{23}) + m_\chi^2 C_0 \right\} (\chi, s_i, \chi; q - p, p) \\ &\quad \left. - \sum_i \left(-\frac{1}{2} + s_W^2 \right) |V_{2i}|^2 (B_0 + B_1)(s_i, \chi; p) \right], \quad (3.40)\end{aligned}$$

$$\begin{aligned}\Delta g_R^\mu &= \frac{y_R^2}{16\pi^2} \left[2 \sum_{ij} \left\{ \left(-\frac{1}{2} - Q_\phi s_W^2 \right) V_{2i}^* V_{2j} - Q_\phi s_W^2 V_{1i}^* V_{1j} \right\} V_{1i} V_{1j}^* C_{24}(s_i, \chi, s_j; p, q - p) \right. \\ &\quad + \sum_i Q_\chi s_W^2 |V_{1i}|^2 \left\{ \frac{1}{2} - 2C_{24} - M_Z^2(C_{12} + C_{23}) + m_\chi^2 C_0 \right\} (\chi, s_i, \chi; q - p, p) \\ &\quad \left. - \sum_i s_W^2 |V_{1i}|^2 (B_0 + B_1)(s_i, \chi; p) \right], \quad (3.41)\end{aligned}$$

$$\begin{aligned}\Delta g_L^{\nu_\mu} &= \frac{y_N^2}{16\pi^2} \left[2 \left(\frac{1}{2} - s_W^2 Q_{\phi_1} \right) C_{24}(\phi_1, \chi, \phi_1; q - p, p) \right. \\ &\quad + Q_\chi s_W^2 \left\{ \frac{1}{2} - 2C_{24} - M_Z^2(C_{12} + C_{23}) + m_\chi^2 C_0 \right\} (\chi, \phi_1, \chi; q - p, p) \\ &\quad \left. - \frac{1}{2} (B_0 + B_1)(\phi_1, \chi; p) \right], \quad (3.42)\end{aligned}$$

where p and q are momenta for muon in $\Delta g_{L,R}^\mu$ (muon neutrino in $\Delta g_L^{\nu_\mu}$) and Z-boson, respectively. Correction to $\mu\nu_\mu W$ -vertex is written by

$$\begin{aligned}\Delta \bar{\delta}_G &= \frac{y_L^2}{8\pi^2} \left[\sum_i |V_{2i}|^2 C_{24}(\phi_1, s_i, \chi; -q, p) \right. \\ &\quad \left. - \frac{1}{4} \left\{ (B_0 + B_1)(\phi_1, \chi; p - q) + \sum_i |V_{2i}|^2 (B_0 + B_1)(s_i, \chi; p) \right\} \right], \quad (3.43)\end{aligned}$$

where p , $p - q$ and q are momenta for muon, muon-neutrino, and W-boson, respectively. Here we use approximation $q^2 = 0$.

In Fig. 11, we show χ^2 contours as a function of m_χ and m_{s_1} in case of (a) $Q_\chi = -1$ and $y_L = -y_R = 0.4$ and (b) $Q_\chi = 0$ and $y_L = y_R = 0.4$. Here we have taken $m_{12}^2 = (50 \text{ GeV})^2$, and $m_{11}^2 = m_{22}^2$. m_{ϕ_1} is chosen so that the χ^2 becomes the smallest, provided that $m_{\phi_1} > 105 \text{ GeV}$ for $Q_\chi = -1$ and $m_{\phi_1} > 46 \text{ GeV}$ for $Q_\chi = 0$ respectively. In both cases shown in Fig. 11, the χ^2 can be as small as 22, which is smaller than those in the previous case where only right-handed muon has new Yukawa coupling. As seen from Fig. 11, the relatively light

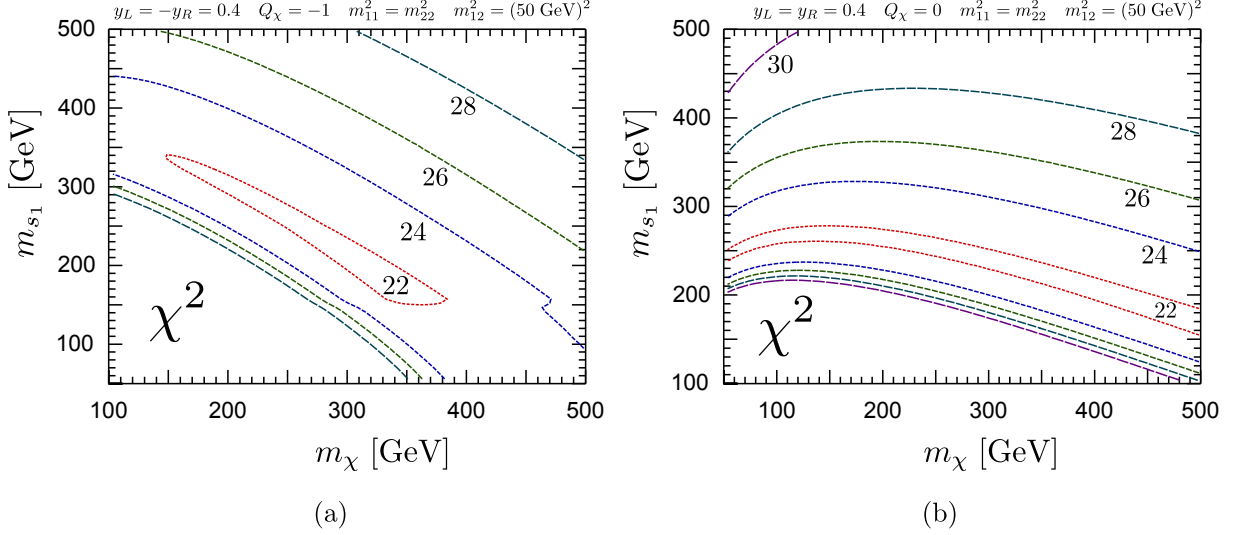


Figure 11: χ^2 contours as a function of m_χ and m_{s_1} in case of (a) $Q_\chi = -1$ and $y_L = -y_R = 0.4$ and (b) $Q_\chi = 0$ and $y_L = y_R = 0.4$. Here we take $m_{11}^2 = m_{22}^2$ and $m_{12}^2 = (50 \text{ GeV})^2$.

χ and s_i are favored by the EW observables. In Table. 1, we show the predicted values of the EW observables in case of $Q_\chi = 0$, $m_{\phi_1} = 300 \text{ GeV}$, $m_\chi = 200 \text{ GeV}$, $m_{11}^2 = m_{22}^2 = (250)^2 \text{ GeV}^2$, and $m_{12}^2 = (50)^2 \text{ GeV}^2$. As shown in Table. 1, the fit is quite good. Therefore, it will be important to know what kind of effects we expect from these particles at the LHC. In a next section, we will discuss the possible effects of these new particles at the LHC.

4 Phenomenology at the LHC

In the previous section, we show that in order to explain the anomaly of muon g-2, it is strongly suggested that there should be the EW scale new particles. It is also suggested that multi-charged particles may be favored by the anomaly of muon g-2. Therefore, these particles may be reachable directly and/or indirectly at the LHC. Here we discuss the effects of these new particles in the Higgs decay $h \rightarrow \gamma\gamma$ and their direct productions at the LHC.

4.1 $h \rightarrow \gamma\gamma$

The SU(2) singlet and doublet scalars can couple to the Higgs boson through the following scalar interactions:

$$\begin{aligned} \mathcal{L} = & -\kappa_1 \phi^\dagger \phi (H^\dagger H) - \kappa_2 (\Phi^\dagger \Phi) (H^\dagger H) - \kappa_3 (H^\dagger \Phi) (\Phi^\dagger H) \\ & - \kappa_4 M \{ (H^\dagger \Phi) \phi^\dagger + \text{h.c.} \}, \end{aligned} \quad (4.44)$$

where H is a standard model Higgs boson doublet. In case where only SU(2) singlet scalar ϕ exists, only coupling κ_1 is non-zero, but in case where both SU(2) singlet ϕ and doublet Φ

scalars are there, all couplings are allowed^{#6}.

In the case where only right-handed muon has new Yukawa interaction, there is SU(2) singlet ϕ , and its interaction with Higgs boson is

$$\mathcal{L} = -\lambda v h \phi^\dagger \phi, \quad (4.45)$$

where $\lambda = \kappa_1$ in this model and v is a vacuum expectation value of Higgs field, $v \simeq 246$ GeV. When Q_ϕ , which is the QED charge of ϕ , is non-zero, ϕ can contribute to the Higgs decay $h \rightarrow \gamma\gamma$. The decay width $\Gamma(h \rightarrow \gamma\gamma)$ is given by

$$\Gamma(h \rightarrow \gamma\gamma) = \frac{\alpha^2 m_h^3}{256\pi^3 v^2} |S(m_h)|^2, \quad (4.46)$$

where the amplitude $S(m_h)$ at leading order is written by

$$S(m_h) = \frac{8}{3}F_t(\tau_t) - F_W(\tau_W) + Q_\phi^2 \lambda \frac{v^2}{2m_\phi^2} F_\phi(\tau_\phi). \quad (4.47)$$

Here the first, the second, and the third terms are top, W, and ϕ contributions, respectively, and $\tau_x = \frac{m_h^2}{4m_x^2}$ ($x = t, W, \phi$). The function F_t , F_W , F_ϕ are given by

$$F_t(\tau) = \tau^{-1} [1 + (1 - \tau^{-1})f(\tau)], \quad (4.48)$$

$$F_W(\tau) = 2 + 3\tau^{-1} + 3\tau^{-1}(2 - \tau^{-1})f(\tau), \quad (4.49)$$

$$F_\phi(\tau_\phi) = \tau^{-1} [-1 + \tau^{-1}f(\tau)], \quad (4.50)$$

where $f(\tau) = \arcsin^2(\sqrt{\tau})$ for $\tau < 1$. Branching ratio of $h \rightarrow \gamma\gamma$ is approximately given by

$$\frac{\text{BR}(h \rightarrow \gamma\gamma)}{\text{BR}(h \rightarrow \gamma\gamma)_{\text{SM}}} \simeq \frac{\Gamma(h \rightarrow \gamma\gamma)}{\Gamma(h \rightarrow \gamma\gamma)_{\text{SM}}} = \left| \frac{\frac{8}{3}F_t(\tau_t) - F_W(\tau_W) + Q_\phi^2 \lambda \frac{v^2}{2m_\phi^2} F_\phi(\tau_\phi)}{\frac{8}{3}F_t(\tau_t) - F_W(\tau_W)} \right|^2, \quad (4.51)$$

because the total decay width does not change much, even if $\Gamma(h \rightarrow \gamma\gamma)$ changes. Here $\text{BR}(h \rightarrow \gamma\gamma)_{\text{SM}}$ and $\Gamma(h \rightarrow \gamma\gamma)_{\text{SM}}$ are the SM predictions at the leading order. Notice that this ratio is a function of m_ϕ and $Q_\phi^2 \lambda$ when Higgs boson mass m_h is fixed. As we discussed earlier, in order to explain the anomaly of muon g-2, larger Q_ϕ may be favored. As can be seen in Eq. (4.51), larger Q_ϕ induces larger effect on $h \rightarrow \gamma\gamma$.

In Fig. 12, the ratio $\Gamma(h \rightarrow \gamma\gamma)/\Gamma(h \rightarrow \gamma\gamma)_{\text{SM}}$ is shown as a function of m_ϕ and $Q_\phi^2 \lambda$. Here we took $m_h = 125$ GeV. As one can see from the figure, the effect can be significant if $Q_\phi^2 \lambda$ is large and m_ϕ is $O(100)$ GeV. For example, as we discussed, when $Q_\phi = 4$, $\lambda = 1$ (-1) and $m_\phi = 200$ GeV, $\Gamma(h \rightarrow \gamma\gamma)/\Gamma(h \rightarrow \gamma\gamma)_{\text{SM}} = 0.12$ (2.7). Unfortunately, we can not predict

^{#6} When the QED charge of ϕ (Q_ϕ) is zero, terms such as $(H^\dagger \Phi)\phi$ and $(H^\dagger \Phi)^2$ are also possible. In our analysis, we assume that such terms are small, for simplicity. Even if we include such terms, our result does not change qualitatively.

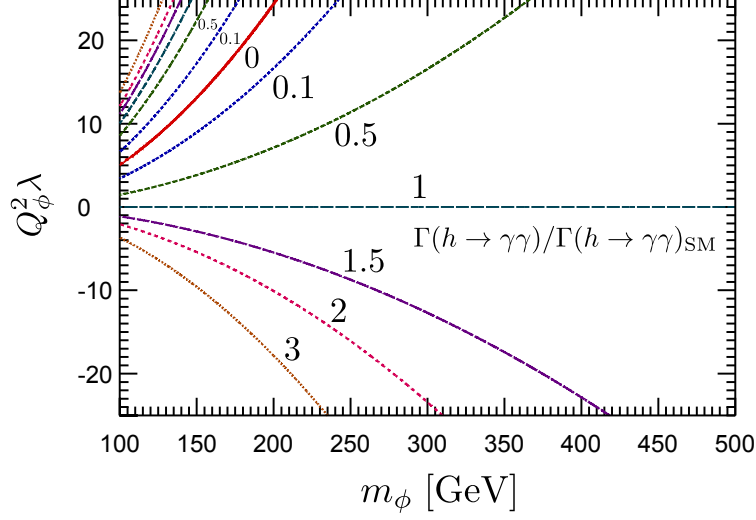


Figure 12: Higgs decay width $h \rightarrow \gamma\gamma$ normalized by the SM prediction $\frac{\Gamma(h \rightarrow \gamma\gamma)}{\Gamma(h \rightarrow \gamma\gamma)_{\text{SM}}}$ as a function of m_ϕ and $Q_\phi^2 \lambda$. Here we take $m_h = 125$ GeV.

the branching ratio $\text{BR}(h \rightarrow \gamma\gamma)$ in this model because λ is unknown. However, it is not surprising that $\text{BR}(h \rightarrow \gamma\gamma)$ is very different from the SM prediction.

In the case where both right- and left-handed muons have new Yukawa interactions, the SU(2) singlet and doublet scalars have interactions with Higgs boson, as shown in Eq. (4.44) and they generate the following interactions:

$$\mathcal{L} = -\kappa_2 v h \phi_1^* \phi_1 - \sum_{ij} \lambda_{ij} v h s_i^* s_j, \quad (4.52)$$

where

$$\lambda_{ij} = \kappa_1 V_{1i}^* V_{1j} + (\kappa_2 + \kappa_3) V_{2i}^* V_{2j} + \frac{M}{\sqrt{2}v} \kappa_4 (V_{1i}^* V_{2j} + V_{2i}^* V_{1j}). \quad (4.53)$$

They contribute to the decay width of $h \rightarrow \gamma\gamma$,

$$\begin{aligned} & \frac{\text{BR}(h \rightarrow \gamma\gamma)}{\text{BR}(h \rightarrow \gamma\gamma)_{\text{SM}}} \\ & \simeq \left| \frac{\frac{8}{3} F_t(\tau_t) - F_W(\tau_W) + Q_1^2 \kappa_2 \frac{v^2}{2m_{\phi_1}^2} F_\phi(\tau_{\phi_1}) + Q_2^2 \sum_i \lambda_{ii} \frac{v^2}{2m_{s_i}^2} F_\phi(\tau_{s_i})}{\frac{8}{3} F_t(\tau_t) - F_W(\tau_W)} \right|^2. \end{aligned} \quad (4.54)$$

When $Q_\chi = -1$, which corresponds to $Q_1 = 1$ and $Q_2 = 0$ (as an example we discussed above), only ϕ_1 can contribute to $h \rightarrow \gamma\gamma$, because s_i does not couple to photon. The result is same as one in Fig. 12 for $\lambda = \kappa_2$ and $Q_\phi = Q_1 = 1$. In this case, the effect

can be significant if κ_2 is large. For example, when $m_{\phi_1} = 250$ GeV and $\kappa_2 = 1$ and -1 , $\Gamma(h \rightarrow \gamma\gamma)/\Gamma(h \rightarrow \gamma\gamma)_{\text{SM}} = 0.95$ and 1.05 , respectively.

When $Q_\chi = 0$, which corresponds to $Q_1 = 0$ and $Q_2 = -1$, scalars s_i ($i = 1, 2$) can contribute to $h \rightarrow \gamma\gamma$. Similarly to the previous case, if the Higgs couplings λ_{11} and λ_{22} are large, the effect on $h \rightarrow \gamma\gamma$ can be significant. For example, when $m_{11}^2 = m_{22}^2$ and $M = \frac{v}{\sqrt{2}}$, we obtain $\lambda_{11} = \kappa$ and $\lambda_{22} = 2\kappa$ for $\kappa_i = \kappa > 0$ ($i = 1 - 4$), on the other hand, $\lambda_{11} = 2\kappa$ and $\lambda_{22} = \kappa$ for $\kappa_i = \kappa < 0$ ($i = 1 - 4$). As a result, for $m_{11}^2 = m_{22}^2 = (300 \text{ GeV})^2$, $\Gamma(h \rightarrow \gamma\gamma)/\Gamma(h \rightarrow \gamma\gamma)_{\text{SM}} = 0.90$ and 1.14 for $\kappa = 1$ and -1 (0.71 and 1.56 for $\kappa = 2$ and -2), respectively. Although it is difficult to predict the decay branching ratio of $h \rightarrow \gamma\gamma$ in this model because it depends on many unknown parameters in scalar interactions, it is possible to have large effect on $h \rightarrow \gamma\gamma$ process.

4.2 Direct productions at the LHC

As we have discussed in the previous sections, the anomaly of muon g-2 strongly suggests the existence of EW scale new particles. Models we discussed in this paper may not be complete, namely, there may be other new particles in the complete models. Therefore, in this paper, we can not discuss the well-defined signatures at the LHC. However, we think that it is important to know how many events of new particles can be generated at the LHC. Here we present the production cross sections of new particles at the LHC.

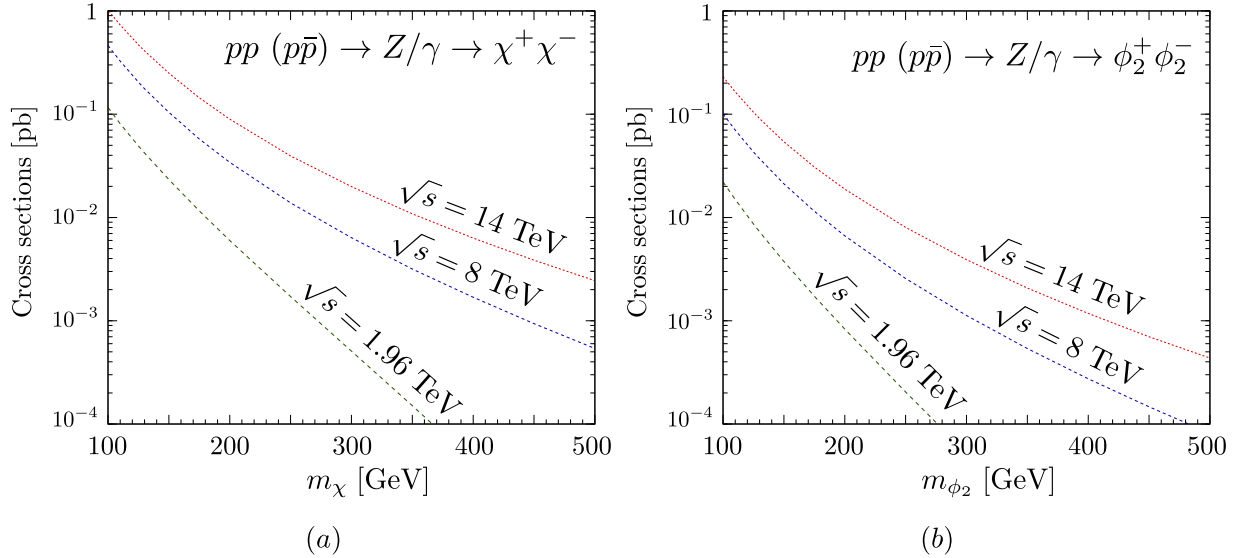


Figure 13: Pair production cross sections of (a) χ in case of $Q_\chi = -1$: $pp(p\bar{p}) \rightarrow Z/\gamma \rightarrow \chi^+ \chi^-$, and (b) ϕ_2^- in case of $Q_2 = -1$: $pp(p\bar{p}) \rightarrow Z/\gamma \rightarrow \phi_2^+ \phi_2^-$ at the LHC (Tevatron), as a function of m_χ and m_{ϕ_2} , respectively. Here we take $\sqrt{s} = 8$ TeV and 14 TeV for LHC and 1.96 TeV for Tevatron.

In the case where the right-handed muon has new Yukawa coupling, singlet scalar (ϕ) and

singlet fermion (χ) exist in the model. When $Q_\chi = -1$, only χ couples to the standard model gauge bosons (Z and γ) because $Q_\phi = 0$. Therefore, the fermion χ can be pair-produced via EW gauge interactions. We calculate the pair production cross section of χ at the LHC ($\sqrt{s} = 8$ TeV and 14 TeV) and at Tevatron ($\sqrt{s} = 1.96$ TeV) as a function of m_χ , as shown in Fig. 13(a). To calculate the production cross sections, we have used the MadGraph [19]. In order to explain the anomaly of muon g-2, the mass of the fermion χ should be of order of about 100 GeV. From Fig. 13(a), the production cross section of χ is in the range of 0.5-0.0005 pb (1-0.001 pb) for $m_\chi = 100 - 500$ GeV and $\sqrt{s} = 8$ TeV ($\sqrt{s} = 14$ TeV) at the LHC and also 0.1-0.001 pb for $m_\chi = 100 - 250$ GeV and $\sqrt{s} = 1.96$ TeV at the Tevatron. If we consider a luminosity of 10 fb^{-1} for $\sqrt{s} = 8$ TeV and 14 TeV, the number of events produced at the LHC is of order of 5-5000 and 10-10000, respectively. Therefore, number of signal events can be significant. In this case, if ϕ is lighter than χ , χ can decay to μ and ϕ . If ϕ is a stable neutral particle, the final signature may be a $\mu^+\mu^- + \text{missing energy}$. This will suffer from the standard model background such as $W^+W^- (\rightarrow \mu^+\mu^-)$ production whose production rate is about 0.29 (0.51) pb for $\sqrt{s} = 8$ TeV (14 TeV) at the LHC. Therefore, the detail study will be very important to discuss the discovery potential of such a signal event. However, the detail signature will depend on the particle spectrum in the complete model. Thus we will leave the detail study. If we consider multi-charged χ , the cross section increases by a factor Q_χ^2 , and the cross section further becomes larger, and hence the constraints from the LHC will be very important. ^{#7}

In the second model where one has a $SU(2)_L$ doublet scalar in addition to ϕ and χ , the scalars can be pair-produced via EW gauge interaction. For example, Fig. 13 (b) shows the production cross sections for the charged $\phi_2^+\phi_2^-$ scalars as a function of m_{ϕ_2} in case of $Q_\chi = 0$, which corresponds to $Q_1 = 0$ and $Q_2 = -1$. We show the predicted values for $\sqrt{s} = 8$ TeV and 14 TeV at the LHC and $\sqrt{s} = 1.96$ TeV at the Tevatron. As can be seen from the figure, the cross sections are in the range of 0.1-0.0001 pb (0.2-0.0005 pb) for $m_{\phi_2} = 100 - 500$ GeV at $\sqrt{s} = 8$ TeV ($\sqrt{s} = 14$ TeV) and also 0.02-0.0001 pb for $m_{\phi_2} = 100 - 250$ GeV at the Tevatron. For simplicity, we have assumed that there are no ϕ - ϕ_2 scalar mixing. In this case, $\phi_1 + \phi_2$ are also produced via W -boson. If masses of $SU(2)_L$ doublet scalar are degenerated, we have checked that the cross section is similar to one in Fig. 13 (b). In general, the signal events have the form $pp (p\bar{p}) \rightarrow V \rightarrow \phi_i^*\phi_j$ where $V = Z, \gamma, W$ and $i, j = 1, 2$. Therefore, Fig. 13 shows the typical values of the cross section in this model.

Although we can not discuss the complete signatures because our sample models are not complete, we stress that the searches for the production processes of these new particles via EW interactions are very important in models where the anomaly of muon g-2 can be explained by these new particles.

^{#7}In addition, ϕ pair production is also not negligible in this case.

5 Summary

The current LHC experiment does not show any deviation from the SM predictions. This result puts severe constraints on new physics models. Especially, colored particles are strongly constrained since the LHC as a hadron collider can easily produce the colored particles via QCD interactions. For example, in the constrained minimal supersymmetric standard model (CMSSM), gluino as well as the first and the second generation squarks are strongly constrained and their typical lower mass limits are about 1 TeV [20]. Therefore, models motivated by the hierarchy problem are getting more constrained, and especially CMSSM as a solution to the hierarchy problem is strongly disfavored.

If we motivate new physics models from the reported anomaly of muon $g-2$, our naive expectation is the existence of EW scale new particles because the size of anomaly of muon $g-2$ is as large as one induced by EW gauge bosons in the SM. In this paper, we analyzed two examples, where muon has new Yukawa type interactions with new particles. One example was a model where right-handed muon has new Yukawa interaction with SU(2) singlet scalar and fermion. In this case, in order to explain the anomaly of muon $g-2$ as well as to satisfy the precision EW measurements, we found that the relatively large new Yukawa coupling and EW scale new particles are strongly favored. We also noted that the multi-charged particles (whose QED charges are large) are favored.

Another example we analyzed was a model where both right- and left-handed muons have new Yukawa interactions with SU(2) doublet scalar and singlet scalar and fermion, so that the chirality flip of muon can occur in the internal fermion line of 1-loop muon $g-2$ diagrams. In this case, new contributions to muon $g-2$ are enhanced, and hence even smaller new Yukawa couplings can explain the anomaly of muon $g-2$. We also showed that the EW observables are also well-fitted by the new physics contributions. In this case, the EW scale new particles are favored by the data.

Although these two examples may be only a part of complete models, the muon $g-2$ as well as the EW observables can constrain the QED charge of new particles as well as the scale of new particles and the size of new Yukawa couplings. Since the EW scale new particles can explain the anomaly of muon $g-2$ and they can be consistent with the precision EW measurements, it is important to study the possible phenomenology at the LHC.

Since some of new particles have QED charges as well as couplings with Higgs boson, the branching ratio of $h \rightarrow \gamma\gamma$ can be effected. Especially, as we showed, multi-charged particles favored by the muon $g-2$ can significantly contribute to $h \rightarrow \gamma\gamma$, and the effects can be sizable. Therefore, Higgs physics will have an impact on models we discussed here.

We also computed direct production cross sections of new particles motivated by the muon $g-2$. Since models discussed here may not be complete, we could not discuss the complete signatures for the models. However, since the number of signal events are not negligible, there may be possibility to reveal new physics models for muon $g-2$ at the LHC. Since we do not need the colored particles to explain the anomaly of muon $g-2$, the search for new particles which only have EW interactions will be very important.

Finally, we comment on the possible completions of models discussed in this paper. The

structure of the model where both right- and left-handed muons have new Yukawa type interactions is quite similar to that of the minimal supersymmetric standard model. When $Q_2 = -1$, the scalar ϕ_2 in SU(2) doublet scalar Φ and SU(2) singlet scalar ϕ correspond to left- and right-handed smuons, respectively. The SU(2) singlet fermion χ is a Bino, for example. A part of a model discussed in Ref. [21], which is motivated by neutrino mass and dark matter is also similar to the model we discussed here. Therefore, our approach can capture crucial features of new physics models for the anomaly of muon g-2 and hopefully create an interesting way to find the physics beyond the standard model.

Note added

After we completed this work, we learned that ATLAS and CMS collaboration at LHC observed a new particle consistent with the SM Higgs boson at a mass of about 125 GeV [22]. Since we have taken the Higgs boson mass to be 125 GeV in our analysis, our conclusion does not change.

Acknowledgments

This work is supported in part by Grant-in-Aid for Scientific research from the Ministry of Education, Science, Sports, and Culture (MEXT), Japan, No. 22540273 (KT). This work is also supported in part by Grant-in-Aid for Nagoya University Global COE Program, “Quest for Fundamental Principles in the Universe: from Particles to the Solar System and the Cosmos”, from the MEXT, Japan.

A Useful function

In this paper, Passarino-Veltman functions [9] are defined by

$$A(A) = 16\pi^2 \mu^{2\epsilon} \int \frac{d^n k}{i(2\pi)^n} \frac{1}{k^2 - m_A^2 + i\epsilon}, \quad (\text{A.1})$$

$$\begin{aligned} B_0(A, B; p) &= 16\pi^2 \mu^{2\epsilon} \int \frac{d^n k}{i(2\pi)^n} \frac{1}{[k^2 - m_A^2 + i\epsilon][(k+p)^2 - m_B^2 + i\epsilon]}, \\ p^\mu B_1(A, B; p) &= 16\pi^2 \mu^{2\epsilon} \int \frac{d^n k}{i(2\pi)^n} \frac{k^\mu}{[k^2 - m_A^2 + i\epsilon][(k+p)^2 - m_B^2 + i\epsilon]}, \\ p^\mu p^\nu B_{21}(A, B; p) &+ g^{\mu\nu} B_{22}(A, B; p) \\ &= 16\pi^2 \mu^{2\epsilon} \int \frac{d^n k}{i(2\pi)^n} \frac{k^\mu k^\nu}{[k^2 - m_A^2 + i\epsilon][(k+p)^2 - m_B^2 + i\epsilon]}, \end{aligned} \quad (\text{A.2})$$

$$\begin{aligned} &C_0(A, B, C; p_1, p_2) \\ &= 16\pi^2 \mu^{2\epsilon} \int \frac{d^n k}{i(2\pi)^n} \frac{1}{[k^2 - m_A^2 + i\epsilon][(k+p_1)^2 - m_B^2 + i\epsilon][(k+p_1+p_2)^2 - m_C^2 + i\epsilon]}, \\ &(p_1^\mu C_{11} + p_2^\mu C_{12})(A, B, C; p_1, p_2) \\ &= 16\pi^2 \mu^{2\epsilon} \int \frac{d^n k}{i(2\pi)^n} \frac{k^\mu}{[k^2 - m_A^2 + i\epsilon][(k+p_1)^2 - m_B^2 + i\epsilon][(k+p_1+p_2)^2 - m_C^2 + i\epsilon]}, \\ &\{(p_1^\mu p_1^\nu C_{21} + p_2^\mu p_2^\nu C_{22} + (p_1^\mu p_2^\nu + p_1^\nu p_2^\mu) C_{23} + g^{\mu\nu} C_{24})\}(A, B, C; p_1, p_2) \\ &= 16\pi^2 \mu^{2\epsilon} \int \frac{d^n k}{i(2\pi)^n} \frac{k^\mu k^\nu}{[k^2 - m_A^2 + i\epsilon][(k+p_1)^2 - m_B^2 + i\epsilon][(k+p_1+p_2)^2 - m_C^2 + i\epsilon]}, \end{aligned} \quad (\text{A.3})$$

where we use dimensional regularization in $4 - 2\epsilon$ dimensions.

For convenience, we list explicit forms of some of above functions.

$$A(m^2) = m^2 \left(\frac{1}{\Delta} + 1 - \log \frac{m^2}{\mu^2} \right), \quad (\text{A.4})$$

$$B_0(A, B; p) = \frac{1}{\Delta} - \int_0^1 dx \log \frac{m_1^2(1-x) + m_2^2 x - p^2 x(1-x) - i\epsilon}{\mu^2}, \quad (\text{A.5})$$

$$B_1(A, B; p) = -\frac{1}{2\Delta} + \int_0^1 dx x \log \frac{m_1^2(1-x) + m_2^2 x - p^2 x(1-x) - i\epsilon}{\mu^2}, \quad (\text{A.6})$$

$$B_{21}(A, B; p) = \frac{1}{3\Delta} - \int_0^1 dx x^2 \log \frac{m_1^2(1-x) + m_2^2 x - p^2 x(1-x) - i\epsilon}{\mu^2}, \quad (\text{A.7})$$

$$\begin{aligned} B_{22}(A, B; p) &= \frac{1}{4}(m_1^2 + m_2^2 - \frac{p^2}{3}) \left(\frac{1}{\Delta} + 1 \right) \\ &- \frac{1}{2} \int_0^1 dx \{m_1^2(1-x) + m_2^2 x - p^2 x(1-x)\} \log \frac{m_1^2(1-x) + m_2^2 x - p^2 x(1-x) - i\epsilon}{\mu^2}, \end{aligned} \quad (\text{A.8})$$

where $\frac{1}{\Delta} = \frac{1}{\epsilon} - \gamma + \log 4\pi$.

References

- [1] G. Aad *et al.* [ATLAS Collaboration], Phys. Lett. B **710**, 49 (2012) [arXiv:1202.1408]; S. Chatrchyan *et al.* [CMS Collaboration], arXiv:1202.1488.
See also recent Tevatron result; [TEVNPH (Tevatron New Phenomina and Higgs Working Group) and CDF and D0 Collaborations], arXiv:1203.3774.
- [2] K. Nakamura *et al.* [Particle Data Group Collaboration], J. Phys. G G **37**, 075021 (2010); B. L. Roberts, Chin. Phys. C **34**, 741 (2010) [arXiv:1001.2898].
- [3] K. Hagiwara *et al.*, J. Phys. G G **38**, 085003 (2011) [arXiv:1105.3149]. See also F. Jegerlehner and A. Nyffeler, Phys. Rept. **477**, 1 (2009) [arXiv:0902.3360]; M. Davier *et al.*, Eur. Phys. J. C **71**, 1515 (2011) [Erratum-ibid. C **72**, 1874 (2012)] [arXiv:1010.4180]; F. Jegerlehner and R. Szafron, Eur. Phys. J. C **71**, 1632 (2011) [arXiv:1101.2872]; T. Teubner *et al.*, AIP Conf. Proc. **1343**, 340 (2011); Nucl. Phys. Proc. Suppl. **218**, 225 (2011).
- [4] T. Aoyama *et al.*, arXiv:1205.5370; arXiv:1205.5368; R. Boughezal and K. Melnikov, Phys. Lett. B **704**, 193 (2011) [arXiv:1104.4510]; A. E. Dorokhov, A. E. Radzhabov and A. S. Zhevlakov, Eur. Phys. J. C **71**, 1702 (2011) [arXiv:1103.2042]; T. Goecke, C. S. Fischer and R. Williams, Phys. Rev. D **83**, 094006 (2011) [arXiv:1012.3886]; Eur. Phys. J. A **47**, 28 (2011) [arXiv:1009.5297]; A. Nyffeler, Chin. Phys. C **34**, 705 (2010) [arXiv:1001.3970]; A. Nyffeler, Phys. Rev. D **79**, 073012 (2009) [arXiv:0901.1172]; D. K. Hong and D. Kim, Phys. Lett. B **680**, 480 (2009) [arXiv:0904.4042]; J. Prades, E. de Rafael and A. Vainshtein, [arXiv:0901.0306]; A. E. Dorokhov and W. Broniowski, Phys. Rev. D **78**, 073011 (2008) [arXiv:0805.0760]; J. Bijnens and J. Prades, Mod. Phys. Lett. A **22**, 767 (2007) [hep-ph/0702170]; M. Hayakawa *et al.*, PoS LAT **2005**, 353 (2006) [hep-lat/0509016]; K. Melnikov and A. Vainshtein, Phys. Rev. D **70**, 113006 (2004) [hep-ph/0312226]; J. H. Kuhn, A. I. Onishchenko, A. A. Pivovarov and O. L. Veretin, Phys. Rev. D **68**, 033018 (2003) [hep-ph/0301151]; T. Kinoshita and M. Nio, Phys. Rev. Lett. **90**, 021803 (2003) [hep-ph/0210322]; M. J. Ramsey-Musolf and M. B. Wise, Phys. Rev. Lett. **89**, 041601 (2002) [hep-ph/0201297]; J. Bijnens, E. Pallante and J. Prades, Nucl. Phys. B **626**, 410 (2002) [hep-ph/0112255]; Nucl. Phys. B **474**, 379 (1996) [hep-ph/9511388]; J. Bijnens, E. Pallante and J. Prades, Phys. Rev. Lett. **75**, 1447 (1995) [Erratum-ibid. **75**, 3781 (1995)] [hep-ph/9505251]; I. R. Blokland, A. Czarnecki and K. Melnikov, Phys. Rev. Lett. **88**, 071803 (2002) [hep-ph/0112117]; M. Knecht, A. Nyffeler, M. Perrottet and E. de Rafael, Phys. Rev. Lett. **88**, 071802 (2002) [hep-ph/0111059]; M. Knecht and A. Nyffeler, Phys. Rev. D **65**, 073034 (2002) [hep-ph/0111058]; Z. Bern, A. De Freitas, L. J. Dixon, A. Ghinculov and H. L. Wong, JHEP **0111**, 031 (2001) [hep-ph/0109079]; M. Hayakawa and T. Kinoshita, Phys. Rev. D **57**, 465 (1998) [Erratum-ibid. D **66**, 019902 (2002)] [hep-ph/9708227]; M. Hayakawa, T. Kinoshita and A. I. Sanda, Phys. Rev. D **54**, 3137

- (1996) [hep-ph/9601310]; M. Hayakawa, T. Kinoshita and A. I. Sanda, Phys. Rev. Lett. **75**, 790 (1995) [hep-ph/9503463].
- [5] T. Moroi, Phys. Rev. D **53**, 6565 (1996) [Erratum-ibid. D **56**, 4424 (1997)] [hep-ph/9512396].
- [6] G. C. McLaughlin and J. N. Ng, Phys. Lett. B **493**, 88 (2000) [hep-ph/0008209].
- [7] S. R. Choudhury, A. S. Cornell, A. Deandrea, N. Gaur and A. Goyal, Phys. Rev. D **75**, 055011 (2007) [hep-ph/0612327].
- [8] K. Kannike, M. Raidal, D. M. Straub and A. Strumia, JHEP **1202**, 106 (2012) [arXiv:1111.2551]; H. Davoudiasl, H. -S. Lee and W. J. Marciano, arXiv:1205.2709.
- [9] G. 't Hooft and M. J. G. Veltman, Nucl. Phys. B **153**, 365 (1979); G. Passarino and M. J. G. Veltman, Nucl. Phys. B **160**, 151 (1979).
- [10] G. -C. Cho *et al.*, JHEP **1111**, 068 (2011) [arXiv:1104.1769].
- [11] G. -C. Cho and K. Hagiwara, Nucl. Phys. B **574**, 623 (2000) [hep-ph/9912260].
- [12] K. Hagiwara *et al.*, Z. Phys. C **64**, 559 (1994) [Erratum-ibid. C **68**, 352 (1995)] [hep-ph/9409380].
- [13] M. E. Peskin and T. Takeuchi, Phys. Rev. Lett. **65**, 964 (1990); Phys. Rev. D **46**, 381 (1992).
- [14] G. Altarelli and R. Barbieri, Phys. Lett. B **253**, 161 (1991); G. Altarelli, R. Barbieri and S. Jadach, Nucl. Phys. B **369**, 3 (1992) [Erratum-ibid. B **376**, 444 (1992)]; G. Altarelli, R. Barbieri and F. Caravaglios, Phys. Lett. B **349**, 145 (1995).
- [15] I. Maksymyk, C. P. Burgess and D. London, Phys. Rev. D **50**, 529 (1994) [hep-ph/9306267].
- [16] Tevatron Electroweak Working Group, f. t. C. Collaboration and D. Collaboration, arXiv:1204.0042.
- [17] Tevatron Electroweak Working Group and for the CDF and D0 Collaborations, arXiv:1107.5255.
- [18] See web page: <http://lepewwg.web.cern.ch/LEPEWWG/>
- [19] J. Alwall *et al.*, JHEP **0709**, 028 (2007) [arXiv:0706.2334].
- [20] For example, see G. Aad *et al.* [ATLAS Collaboration], arXiv:1206.1760; S. Chatrchyan *et al.* [CMS Collaboration], arXiv:1206.3949.

- [21] T. Hambye, K. Kannike, E. Ma and M. Raidal, Phys. Rev. D **75**, 095003 (2007) [hep-ph/0609228].
- [22] G. Aad *et al.* [ATLAS Collaboration], [arXiv:1207.7214]; S. Chatrchyan *et al.* [CMS Collaboration], Phys. Lett. B [arXiv:1207.7235].